Master's thesis

Physical Modelling and Automatic Configuration of CES Valve

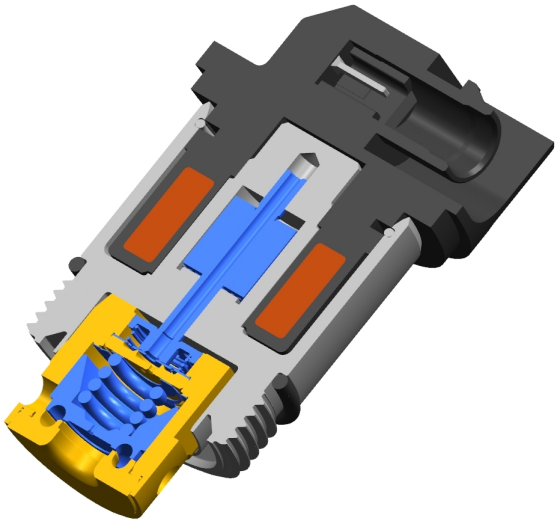

Anders Gällsjö, Mattias Johansson
June 15, 2012

LIU-IEI-TEK-A−12/01305−SE

Abstract

This thesis has been performed at Öhlins Racing AB which is known world-wide for its high quality racing shock absorbers. Öhlins have been developing shock absorbers for more than 30 years and in addition to this they also develop a technology for semi-active suspension.

Semi-active suspension technology makes it possible to achieve an intelligent and dynamic vehicle chassis control. Compared to standard passive suspensions, semi-active dampers allow improving vehicle cornering performance while still providing good comfort when cruising. This is achieved by a real time adjustment of the suspensions damping characteristics.

Öhlins system for semi-active suspension is called CES (Continuously controlled Electronic Suspension). The systems consist of electronically controlled hydraulic valves for uniflow dampers. These valves are mounted on all four dampers of the vehicle and are controlled individually to provide the desired ride quality. The valves are configurable to suit many types of vehicles by changing internal parts.

The first goal of this thesis project was to study the behaviour of the CES valve and uniflow damper. In order to achieve this a simulation model was created using Hopsan which is a 1-dimensional multi-domain modelling tool developed at the division of Fluid and Mechatronic Systems at Linköping University. The model considers mechanical forces from for example springs together with hydraulic forces. It was validated against static and dynamic measurements made in a flow bench and a dynamometer.

The second goal was to use the simulation model as part of a tool that configures the CES valve according to a requirements specification. To achieve this goal a method of estimating the characteristics of the internal damper valves was developed. This estimation method, together with the simulation model, was used to choose the best valve configuration by using weighted least-squares. The result is presented in a Matlab-based graphical user interface.

Preface

This thesis was the final part of our education towards becoming Masters of Science in Mechanical Engineering. It was made as a collaboration between Öhlins Racing AB and Linköping University.

We would like to thank everyone at Öhlins Racing AB in Jönköping for all the help and good advice during our thesis work. We would especially like to thank our mentor Erik Jonsson who has been of great assistance during the entire thesis.

We would also like to thank our mentor at Linköping University, Robert Braun who has given invaluable support throughout the thesis.

Jönköping June 2012

Mattias Johansson and Anders Gällsjö

Contents

List of Figures

1 Introduction

An introduction to this master's thesis is presented in this chapter.

1.1 Background

This thesis has been performed at Öhlins Racing AB which is known for its high quality racing shock absorbers. Öhlins is a well known part of the motorsport industry and have been developing shock absorbers for more than 30 years. In addition to this they also develop a technology for semi-active suspension.

Today there are three main types of suspensions available:

- Conventional suspensions uses a fixed damping coefficient and a big compromise between handling and comfort is necessary. A stiff damper would provide good handling during cornering but an uncomfortable ride while cruising.
- Active suspensions give the best characteristics regarding cornering and comfort since it is able to add energy to the system. This means it can apply an independent force on the suspension to control the movement of the vehicle. The main drawbacks are the complexity of the system and its high energy consumption.
- Semi-active suspensions control the damping coefficient of the suspension but cannot add energy to the system. This means it can control the magnitude of the damping force but not its direction. It removes almost all the compromise between handling and comfort that is found in conventional suspensions. The main advantages compared to active suspensions are the low power consumption and a lower manufacturing cost.

Öhlins system for semi-active suspension is called CES (Continuously controlled Electronic Suspension). The system consists of a solenoid controlled hydraulic valve mounted on a triple tube (uniflow) damper. The CES valve, composed by a pilot stage and a main stage, presents a unique geometrical design and is configurable to suit different types of applications by changing internal parts.

Öhlins Racing AB is interested in using simulations early in the development process to shorten lead times. It is also of importance to increase the knowledge about how simulation tools can be incorporated in the development process. Therefore this master's thesis is performed using Hopsan which is a multi-domain simulation software. Hopsan is developed at Linköping University and is a freeware alternative to other simulation tools, for example AMESim and Dymola.

1.2 Goal of the thesis project

The first goal is to study the behaviour of the CES valve, both alone and coupled with a damper. In order to achieve this a simulation model of the valve and damper will be developed using Hopsan. The second goal is to use the simulation model as part of a tool that configures the CES valve according to a damping specification.

1.3 Boundaries

The dynamometer and flow bench, which are used to make measurements, have already been analysed in [4] and will not be analysed further in this master's thesis. The CES valve can be configured with three different types of main stages, high-flow, normal-flow and high-pressure. Only the high-flow main stage will be modelled in order to fit the task within the extent of a thesis project. The solenoid will be modelled as a static function of the input current.

1.4 Method

The CES valve and damper were studied and then modelled in the simulation program Hopsan. The modelling focused on creating an intuitive model that is easy to understand. The different components were validated separately as far as possible and then validated as a complete model. Technical papers on the subject of modelling hydraulic valves and dampers were studied before development of the simulation models started.

2 Theory

The theory behind some vital elements in this master's thesis is explained in this chapter. All equations are taken from [1] throughout this thesis if nothing else is specified.

2.1 Solenoid

The solenoid consists of an electromagnetically inductive coil that is wound around a movable steel rod. The magnetic field moves the steel rod creating a mechanical force. This force can be controlled by controlling the current in the coil. The force is typically weak but can be controlled directly by changing the current and thus the solenoid has a very short reaction time.

2.2 Turbulent orifice

For a turbulent orifice the flow is proportional to the square root of the pressure difference across the orifice according to equation 2.1. The flow is calculated using the oil density ρ, the flow area A, the pressure difference across the orifice Δp and the flow coefficient Cq. This coefficient varies for different orifice geometries.

$$q = C_q * A * \sqrt{\frac{2}{\rho}|\Delta p|} sign(\Delta p) \tag{2.1}$$

2.3 Laminar orifice

The flow is proportional to the pressure difference over the orifice, Δp, with the proportionality constant K_c according to equation 2.2.

$$q = K_c \Delta p \tag{2.2}$$

2.4 Flow forces

Flow forces are generated when fluids change speed and direction and are calculated according to equation 2.3. The flow forces are calculated using the flow coefficient C_q, the area gradient ω, the stroke length x, the pressure difference across the orifice $(p_1 - p_2)$, the beam angle δ, the oil density ρ, the length l and the flow acceleration $\dot{q}$. The variables ω, x, δ and l describes the geometry of the valve.

$$F_s = |2C_q \omega x (p_1 - p_2) cos(\delta)| + pl\dot{q} \tag{2.3}$$

2.5 Hydraulic cylinder

The hydraulic cylinder component used when modelling takes bulk modulus, dead volumes and viscous friction into account. This component is used to model the poppets in the CES valve. It models leak flow between the piston and the cylinder wall as laminar flow.

2.5.1 Bulk modulus

The bulk modulus, K, of a substance measures the substance's resistance to compression and is defined according to the equation 2.4 where V is the volume and P is the pressure. The bulk modulus affects how mechanical waves propagate through the substance.

$$K = -V\frac{\partial P}{\partial V} \tag{2.4}$$

2.5.2 Viscous friction

Viscous friction is generated due to the viscosity of the oil. When an object, for example a cylinder, is moving through the oil it generates a velocity gradient i.e. different layers of the oil move at different velocities. Viscous friction arises from shear stress between these layers.

2.5.3 Dead volumes

The dead volume in a cylinder is the volume that is left between the piston and the cylinder wall when the cylinder reaches the end of its stroke.

2.6 Flow bench

A flow bench is used to perform measurements on the CES valve. The flow bench consists of a hydraulic pump which supplies the valve with oil and a current source which controls the solenoid. The flow bench controls the flow and the solenoid current while the pressure drop across the valve is measured.

2.6.1 Pq-measurements

During a pressure-flow measurement the flow is ramped up and then down at a number of constant solenoid currents according to figure 2.1.

2.6.2 ASR-measurements

During an Active Step Response measurement the flow is held constant while control current steps are made. Steps to different current levels are made for several different flows according to figure 2.2.

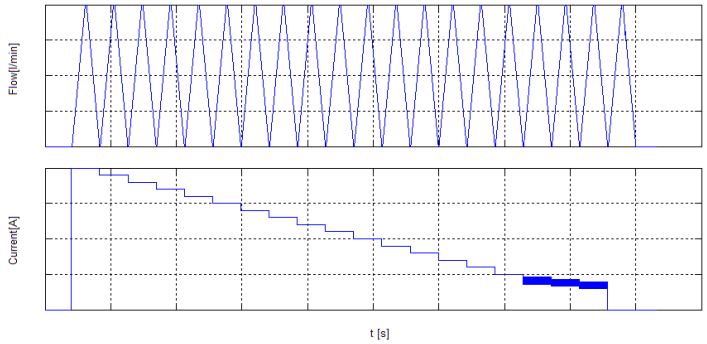

Figure 2.1: Control signal to the valve and flow bench during a Pq-measurement

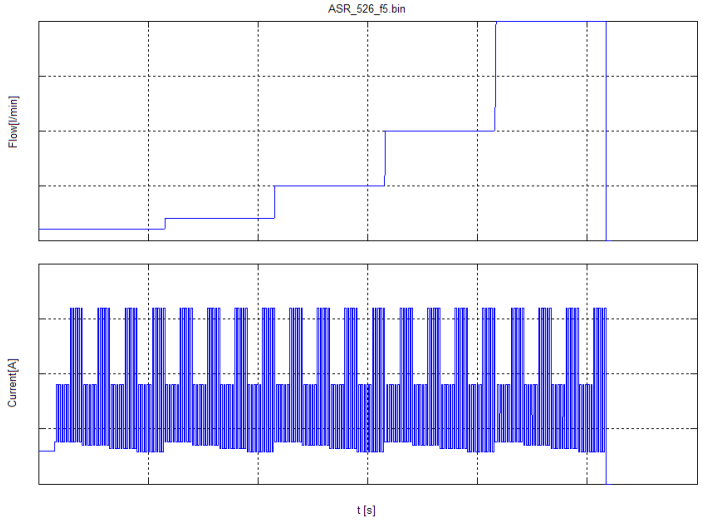

Figure 2.2: Control signal to the valve and flow bench during an ASR-measurement

2.7 Dynamometer

A dynamometer (dyno for short) is used to perform measurements on the damper. The dyno consists of a hydraulic pump which controls a hydraulic cylinder to which a damper is bolted on. The position and force is measured and the velocity is derived from the position.

During dyno measurements the velocity is controlled according to sinusoidal curves where the desired amplitude is set and the frequency is adapted to get a 5 cm stroke. An example of a control sequence is shown in figure 2.3.

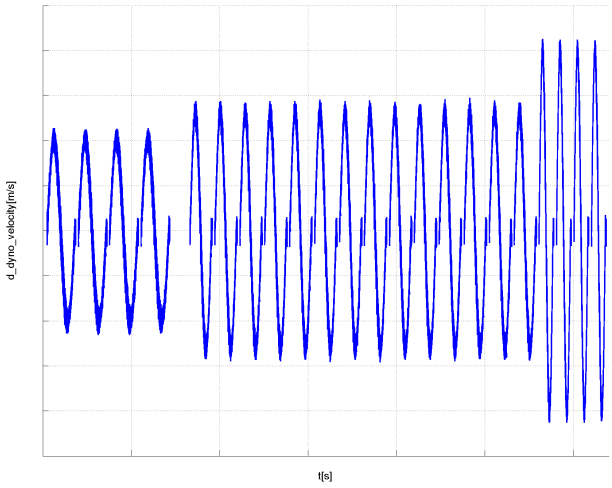

Figure 2.3: Control signal to dynamometer

2.8 Least-squares method

The least-squares method is a way to determine the best fit line to data, in the context of this thesis this means minimizing the sum of squared residuals. A residual is the difference between a observed value and the corresponding value from a model. The different residuals are weighted to give possibility to prioritize between different residuals. The least-squares method is used according to equation 2.5 where W_i is the weight of the residual r_i.

$$S = \sum_{i=1}^{n} W_i r_i^2 \tag{2.5}$$

3 Literature review

Parts of what have been published regarding the CES valve and modelling of valves and dampers is summarized here.

3.1 Studies of the CES valve

The CES valve has been studied in several master's theses, a linear model of the CES valve was made using MATLAB/SIMULINK in [4]. The model could reproduce some step responses but was not good enough for more oscillating step responses. A specific type of oscillations in an older version of the valve was examined in [5] by using a model which was linearised around an operating point. This model could describe parts of the models behaviour but had problems with time delays and dynamics. The models in [4] and [5] were created using basic equations for hydraulics and mechanics. These equations were Laplace transformed and implemented in MATLAB/SIMULINK.

3.2 Modelling of hydraulic valves and dampers

A model of a pilot controlled pressure relief valve was created using bond-graph theory in [6]. The model output fitted well with measurements during dynamic responses. The authors concluded that the preload of the pilot spring and the dampening of the main poppet were important. The model could be improved by using a more detailed model of the solenoid since the implemented one had no dynamics.

A model of a mono-tube damper manufactured by Öhlins Racing was built in [12]. The principle of this damper is fundamentally different from the triple tube damper in this thesis but contains some elements that are similar, for example the check valve in the piston. The author concluded that friction and stiffness of the damper wasn't insignificant. More studies were needed regarding variations in the compressibility of the oil and the dynamics of the check valves.

A parametric model of a mono-tube damper was generated in [7]. The model took hydraulic and mechanical friction forces into account together with pressure from the gas reservoir. The model was fairly simple and could be used for real-time simulations while also giving a model output that was close to measurements. Validation was made using data from a dynamometer and from driving on a racing track. A twin tube damper was modelled in [10] using the Modelica language but wasn't validated against measurements.

Hopsan has previously been used to simulate the cardiovascular system of the human body in [8] and the arterial tree in [9].

4 System overview

An overview of the system which was studied is presented in this chapter.

4.1 System sketch

The system consists of a damper and an externally mounted CES valve. A sketch of the principle function of the damper and valve is shown in 4.1.

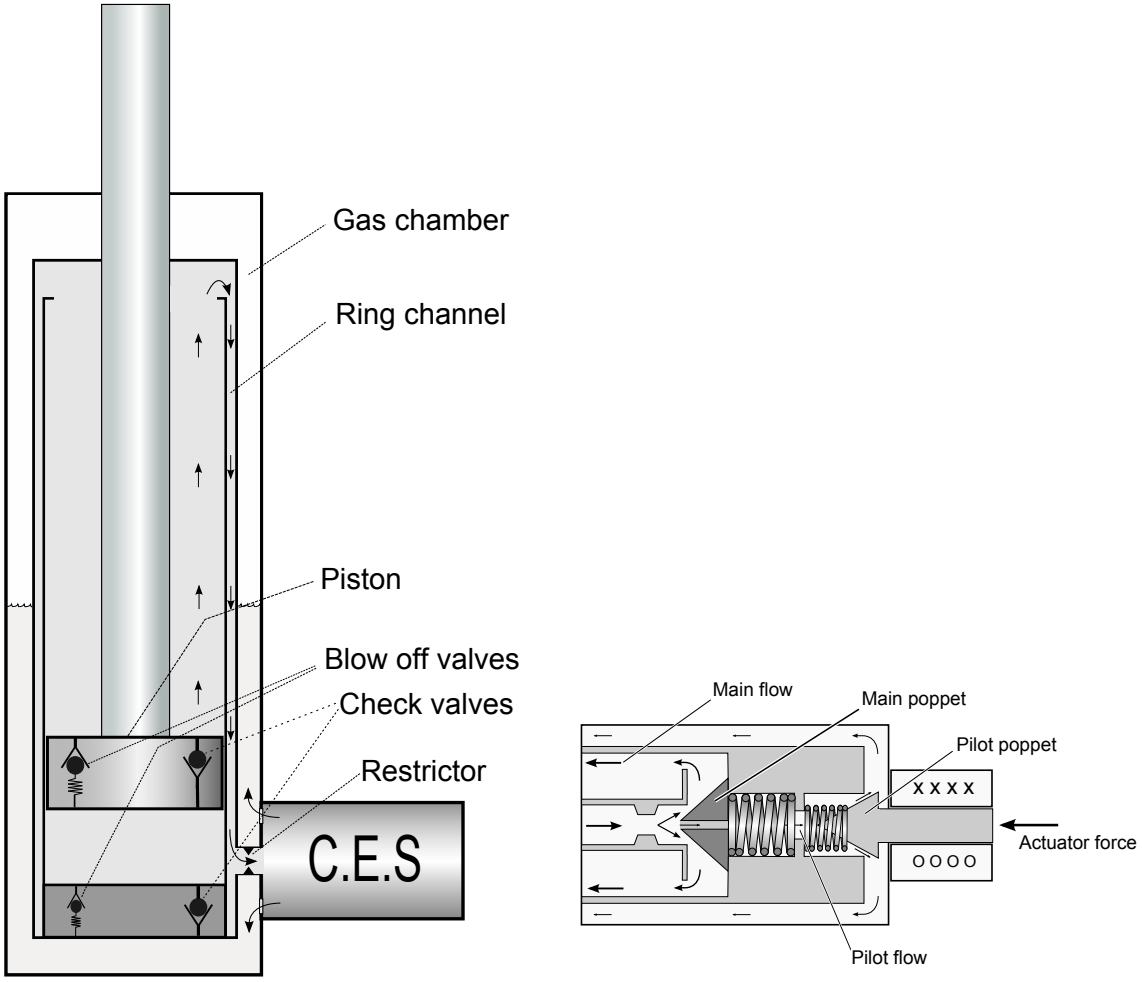

(a) Damper (b) CES valve

Figure 4.1: Sketch of the principle function of the damper and CES-valve.

4.2 Damper

The damper cylinder consists of an outer tube and two inner tubes between which a ring channel is formed. The damper is of the type uniflow which means that the oil will flow in the same direction through the ring channel both during compression and rebound. There is a check valve and a blow-off valve through both the piston and the base according to figure 4.1.

4.2.1 Compression

The direction of a compression stroke is defined as the piston moving downwards in figure 4.1. During a compression stroke the check valve in the piston opens while the blow-off valve in the bottom prevents the pressure from building too high in the chamber below the piston (the compression chamber). This means the oil will flow upwards in the inner tube and down through the ring channel.

4.2.2 Rebound

A rebound stroke is defined as the piston moving upwards in figure 4.1. During a rebound stroke the check valve in the bottom opens and the blow-off valve in the piston prevents the pressure from building too high in the chamber above the piston (the rebound chamber). This means the oil will flow upwards in the inner tube and down through the ring channel. Thus, the oil will flow in the same direction through the CES valve both during compression and rebound.

4.3 CES valve

The CES valve consists of a main stage and a solenoid controlled pilot stage. The pilot stage controls the pressure inside the main poppet which then controls the main flow through the CES valve. The main stage consists of two orifices in series which are designed to open the valve in a smooth and controlled way.

4.3.1 Configuration parameters

The CES valve which was studied can be configured to suit the needs of a customer. The parameters that are changeable are:

- Spring rate of main poppet spring
- Spring rate of pilot stage shim
- Diameter of pilot stage seat
- Type of main stage (High flow, Normal flow, High-pressure)

These parameters are used to get as close as possible to a damping curve which is specified by the customer.

4.4 Hopsan

Modelling of the CES valve and damper was made in a multi-domain simulation program called Hopsan. This program is developed at the department of Fluid and Mechatronic systems at Linköping University. More information about the program can be found in [2] and [3].

5 Modelling

The model of the CES valve and the damper is explained in this chapter.

5.1 System modules

The system was divided into three main modules.

- Pilot stage of the CES valve
- Main stage of the CES valve
- Damper

5.2 Assumptions and simplifications

A number of assumptions and simplifications were made, as shown below, to limit the extent of this thesis.

- All springs in the valve are linear
- Bulk module and oil temperature are constant
- Leak flows are laminar
- Oil flow is either strictly laminar or turbulent

5.3 Properties of the hydraulic oil

The hydraulic oil that was used during measurements was a shock absorber oil with a density of 843 kg/m^3 and viscosity of 20,7 mm^2/s, both at a temperature of 20 °C. The bulk module was assumed to be around 1.4 GPa which is a reasonable value since hydraulic shock oils generally has a bulk module in the range of $1.38 * 10^9$-$2 * 10^9$ Pa according to [11]. It is reasonable to assume that some gas was dissolved in the oil and therefore a value in the lower end was chosen.

5.4 The pilot stage

An orifice through the pilot seat defines the flow into the pilot stage. The pilot poppet is affected by hydraulic and mechanical forces. The mechanical forces consists of the solenoid, a spring and a shim. This shim is hereafter refereed to as the pilot shim. A sketch of the pilot stage is shown in figure 5.1 and a screenshot of the Hopsan model is shown in figure A.1 in Appendix A.

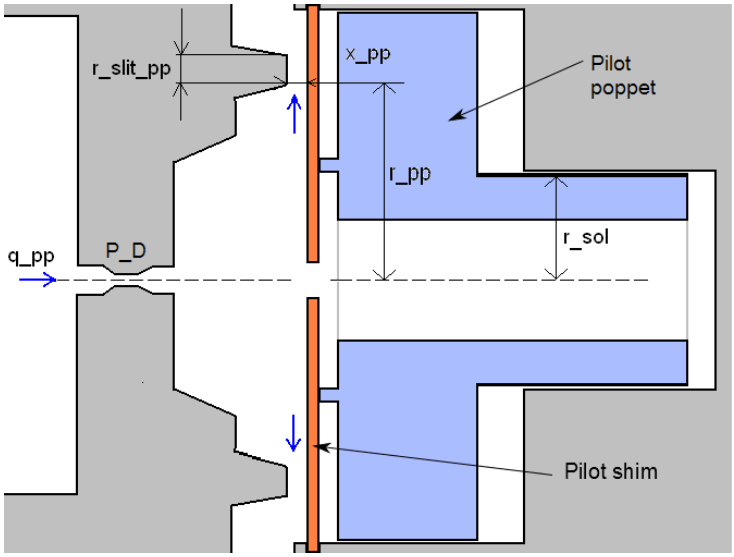

Figure 5.1: Sketch of the pilot stage

5.4.1 Flow through the pilot orifice

The area which the pilot flow goes through is proportional to the position of the pilot poppet, x_{pp}. This position was defined as zero when the pilot stage was completely closed. The flow area, $A_{q_{pp}}$, was therefore calculated using the pilot seat radius and poppet position according to equation 5.1. The flow through the pilot orifice, q_{pp}, was modelled as a turbulent orifice in Hopsan. The flow coefficient, C_q, depends on the geometry of the orifice and changes as a function of the poppet position. This function varies the flow coefficient between 0.4 and 1. The flow coefficient is 0.4 when the pilot orifice is closed and then increases as the orifice opens. Figure 5.2 shows how C_q varies during the stroke. There is also a leak flow from the pilot stage to tank which is modelled as a laminar flow.

$$A_{q_{pp}} = 2\pi r_{pp} x_{pp} \tag{5.1}$$

5.4.2 Pilot poppet

The pilot poppet was modelled as a cylinder attached to a mass. The mass, m_{pp}, includes the poppet and solenoid rod mass. Both sides of the cylinder component are joined together by a lossless connector since the pilot poppet and solenoid rod are hollow. Thus, the pressure on both sides of the cylinder is equal.

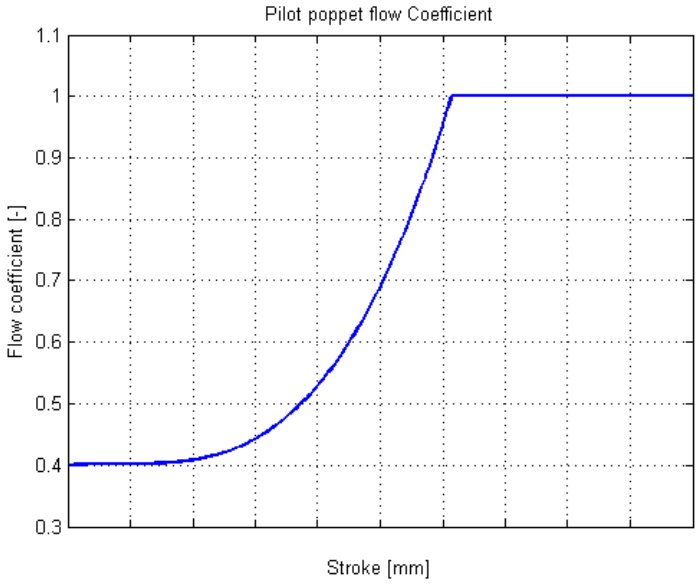

Figure 5.2: Flow coefficient as a function of poppet position (pilot stage)

5.4.3 The pilot orifice

The pilot orifice can be seen as an axial annular slit. The flow through this slit was assumed to be a laminar leak flow when the orifice was closed. The pressure as a function of the radius could then be calculated using equation 5.2. The variable $p_1 - p_0$ is the pressure drop across the orifice while r_1 and r_2 is the inner and outer radius. Figure 5.3 shows that pressure decreases almost linearly across the orifice. Therefore it was initially assumed that half the radius of the slit should be added to the pressurised area in the cylinder component that represented the pilot poppet. This was then tuned to 44.1% of the radius to obtain better agreement with measurements. The hydraulic force on the poppet was calculated according to equation 5.3 and 5.4.

$$p(r) = p_1 - (p_1 - p_0)\frac{ln(\frac{r}{r_1})}{ln(\frac{r_2}{r_1})} \tag{5.2}$$

$$F_{hyd_{pp}} = p_{V_{pp}} A_{pp} \tag{5.3}$$

$$A_{pp} = \pi((r_{pp} + 0.44 r_{slit_{pp}})^2 - r_{sol}^2) \tag{5.4}$$

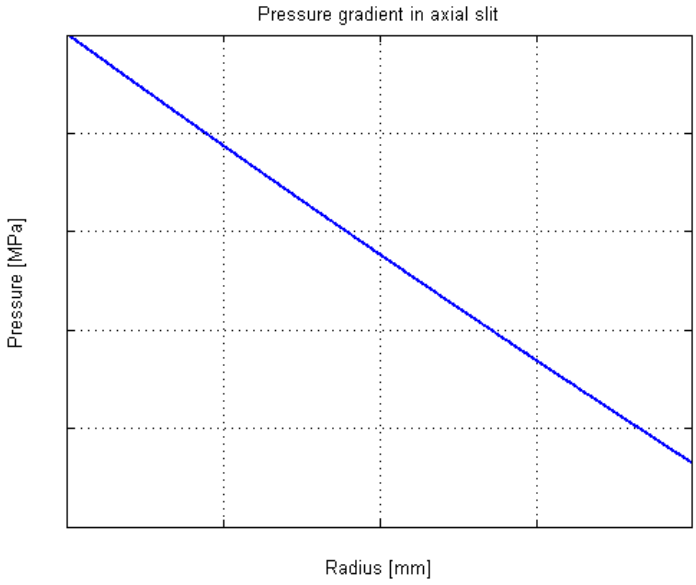

Figure 5.3: Pressure as a function of radius for the pilot orifice

5.4.4 The P_D orifice

This orifice was modelled as a turbulent orifice with a flow coefficient of 0.77.

5.4.5 Solenoid force

The solenoid force at different currents has been measured in a stroke-force meter. The obtained data was used to create a third order polynomial which was necessary since a second order polynomial couldn't represent the solenoid accurately. The output from the polynomial and measured data is shown in figure 5.4 where measured values are marked with circles. The force was assumed to be independent of the position of the solenoid rod and values were taken as an average of 10 measurements. The function that was used for the solenoid force is presented in equation 5.5.

$$F_{sol} = c_1 i_{sol}^3 + c_2 i_{sol}^2 - c_3 i_{sol} \tag{5.5}$$

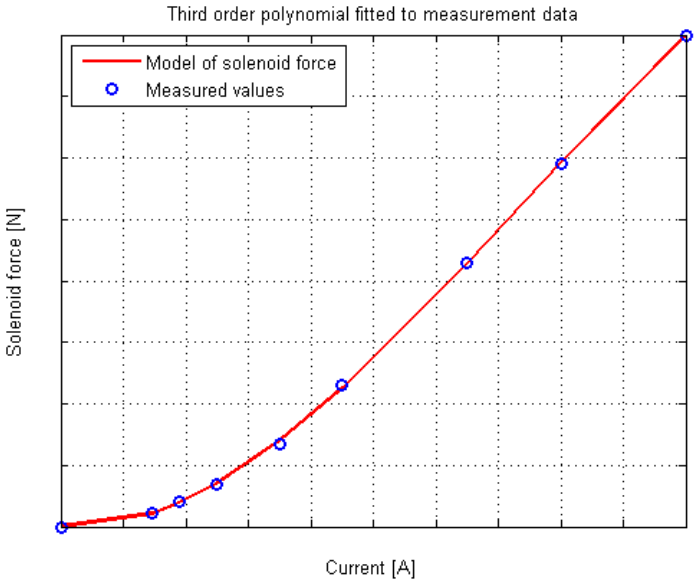

Figure 5.4: Solenoid force as a function of current, third order polynomial

5.4.6 Solenoid friction

The armature of the solenoid is not completely symmetrical in shape. It does therefore produce both radial and axial forces when affected by the magnetic field from the surrounding coil. The radial force creates friction between the armature and its bushings which gives rise to hysteresis. This friction is modelled as a function of current according to equation 5.6.

$$F_{fr,sol} = c_4 i_{sol} \tag{5.6}$$

5.4.7 Flow forces

It is reasonable to assume that some kind of flow forces act on the pilot poppet since the flow makes a significant directional change in the pilot stage. The flow angle was assumed to be 0° since the pilot shim extends radially in the slit. The shim thereby forces the flow to make a 90° change in direction which corresponds to 0° in the flow force equation.

5.5 The main stage

The flow of oil enters the main stage via the restrictor called D_s and is then divided between main flow (q_{mp}) and pilot flow (q_{pp}). The pilot flow enters the inside of the main poppet through the J_D orifice. A sketch of the main stage is shown in figure 5.5 and a screenshot of the Hopsan model is shown in figure A.2 in Appendix A.

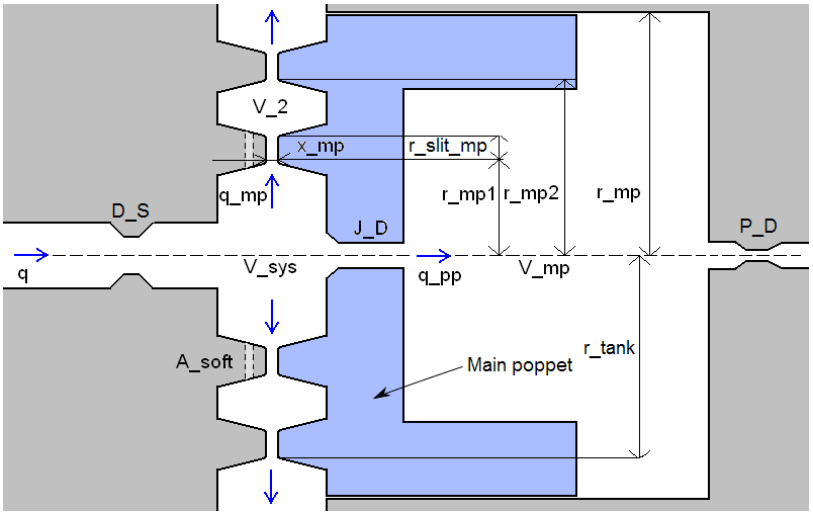

Figure 5.5: Sketch of the main stage

5.5.1 Flow through the main orifice

The main stage consists of two orifices in series which are separated by a donut-shaped volume (V_2). The flow areas of these orifices are proportional to the position of the main poppet and was calculated using equation 5.7 and 5.8. A small slit in the inner orifice, with area A_{soft}, is used to make the valve open softly. This slit between the volumes V_{sys} and V_2 is open even if the main stage is completely closed. The flow through the main orifices and the soft-opening slit was modelled as turbulent.

The flow coefficient, C_q, changes as a function of the poppet position since it changes the geometry during the stroke. The flow coefficient varies linearly between 0.77 and 1 according to figure 5.6.

$$A_{q_{mp_1}} = 2\pi r_{mp_1} x_{mp} + A_{soft} \tag{5.7}$$

$$A_{q_{mp_2}} = 2\pi r_{mp_2} x_{mp} \tag{5.8}$$

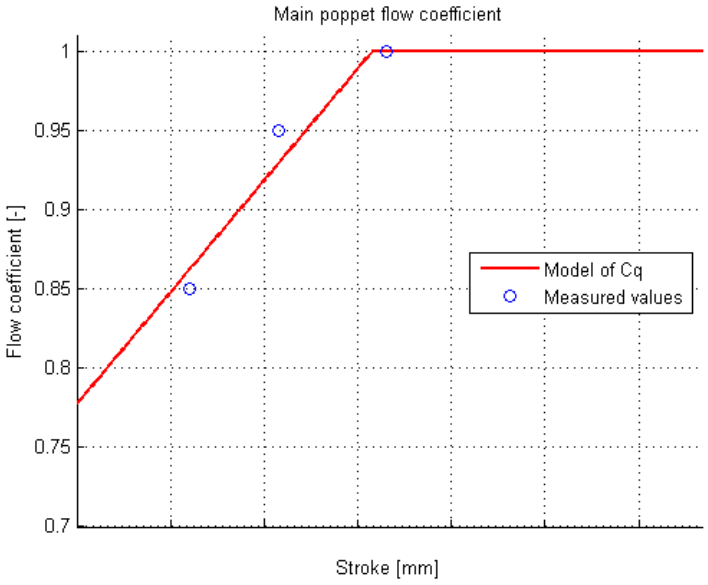

Figure 5.6: Flow coefficient as a function of main poppet position

5.5.2 The main poppet

The main poppet was modelled as a cylinder attached to a mass. The two inner volumes of the cylinder were connected with the J_D orifice. The hydraulic force that affects the main poppet depends on the pressure in the V_{sys}, V_2 and V_{mp} volumes. The hydraulic force was calculated according to equation 5.9 and the pressurised areas by using 5.10, 5.11, 5.12 and 5.13. Half the radial width of the slits were initially added to the radius of the areas but were removed after validation, i.e. the slits are not pressurised. The tank pressure is acting on an annular area outside of the series orifices.

$$F_{hyd_{mp}} = p_{V_{sys}} A_{mp_1} + p_{V_2} A_{mp_2} - p_{V_{mp}} A_{mp} + p_{tank} A_{tank} \tag{5.9}$$

$$A_{mp_1} = \pi r_{mp_1}^2 \tag{5.10}$$

$$A_{mp_2} = \pi (r_{mp_2}^2 - (r_{mp_1} + r_{slit_{mp}})^2) \tag{5.11}$$

$$A_{mp} = \pi r_{mp}^2 \tag{5.12}$$

$$A_{tank} = \pi (r_{mp}^2 - r_{tank}^2) \tag{5.13}$$

The leak flow from the poppet's inner volume (V_{mp}) was simulated with a laminar orifice (equation 2.2) where the flow coefficient of the orifice was calculated using

the tolerances of the poppet and housing. The part of the leak flow due to the velocity of the poppet was neglected since it was small compared to the leak flow due the pressure difference. The coefficient was calculated using equation 5.14. The variable r_{nom} is the nominal radius and h_0 is the narrow gap between the poppet and housing. The poppet is assumed to be centered in the housing.

$$K_c = \frac{\pi r_{nom} h_0^3}{6\eta l_{mp}} \tag{5.14}$$

5.5.3 Flow forces

The flow angle changes as a function of the stroke for the inner of the series orifices in the main stage. The flow angle was assumed to be a linear function of poppet position according to figure 5.7. The flow angle in the outer orifice was kept constant at 70 °.

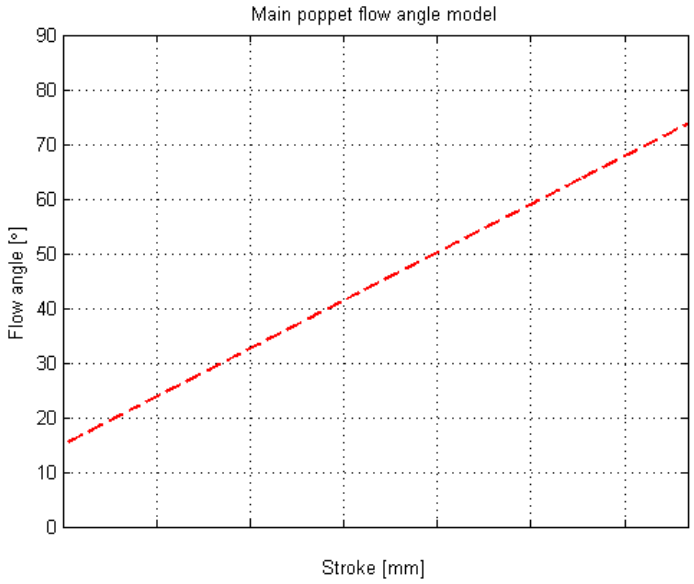

Figure 5.7: Flow angle as a function of main poppet position (inner series orifice)

5.5.4 The J_D and D_s orifices

These orifices were modelled as turbulent with a flow coefficient of 0.85.

5.6 The damper

A damper that was identical to the one used during measurements was cut apart. Diameters and lengths were measured on that specimen using callipers, no tolerances for the different surfaces were known.

5.6.1 Piston and rod

The piston and rod were simulated using a hydraulic cylinder component. The mechanical friction in the damper was neglected. Pressurised areas and stroke length were derived from measurements made with callipers. The viscous friction in the damper was set to 55 Ns/m. The leakage over the piston was assumed to be small compared to the leakage through the check valves and was therefore set to zero.

5.6.2 Blow-off valves

The blow-off function in the piston and base valves were simulated with Hopsan's model of a hydraulic massless poppet valve. The parameters in the poppet model, for example spring stiffness and preload, were tuned to give good agreement with measurement data. A laminar leakage was modelled in parallel with the poppet valve and a check valve was used to prevent the flow from going in the wrong direction. A screenshot off the model of the blow-off in the base is shown in figure A.4 in Appendix A. The other blow-off and the check valves use the same structure but with different parameters in the components.

5.6.3 Check valves

The check valves in the piston and base of the damper were also modelled with massless poppet valves. The main difference was that these valves had a very small opening pressure and were designed to create a very small pressure drop at high flows.

5.6.4 Ring channel and restrictor

The hydraulic flow is forced through two circular holes in the inner tube wall and a restrictor before it reaches the CES valve. The flow coefficient of the two holes and the restrictor was set to 0.67 because their inlets were sharp-edged.

5.6.5 Gas pressure

The gas pressure is assumed to be constant during the length of the stroke. In reality it will be higher when the damper is fully compressed but this is insignificant compared to the uncertainty in the gas pressure measurement. The piston rod is inserted into the damper during the stroke and thereby compresses the gas volume, which increases the tank pressure in the damper.

6 Validation and results

A validation of the results from the CES valve and damper model is presented in this chapter.

6.1 Validation possibilities

The damper can be run in the dyno with a fixed valve and thus the damper can be validated separate from the CES valve. The pilot stage can be run in the flow bench separate from the main stage while the main stage can't be run without a pilot stage. This means the pilot stage can be validated separately but the main stage cannot.

6.2 Validation of the pilot stage model

Pq-measurements were made in the flow bench to validate the model of the pilot stage. The stiffness of the pilot shim and the diameter of the pilot seat were changed between measurements. The extreme cases, which gives the lowest and highest pressure drop, (for example weakest shim with largest pilot diameter)are shown in this report. These measurements were each performed on three separate individuals to rule out any faulty behaviour.

Attempts were made to study the dynamics of the pilot stage through ASR-measurements. These measurements gave unsatisfactory results due to the fact that the flow was low (approximately 2 l/min) and the oil volume in the flow bench was relatively big. Thus the dynamics of the flow bench dominated the measurements.

6.2.1 Solenoid force independent of position

Measurements on the solenoid were studied to determine if the solenoid force could be modelled as independent of armature position. An example of a solenoid measurement is shown in figure 6.1. The working range when mounted in a CES valve is somewhere within the marked boxes and the force is virtually constant throughout the stroke, therefore the solenoid force can be modelled as independent of armature position. The hysteresis is caused by the solenoid friction.

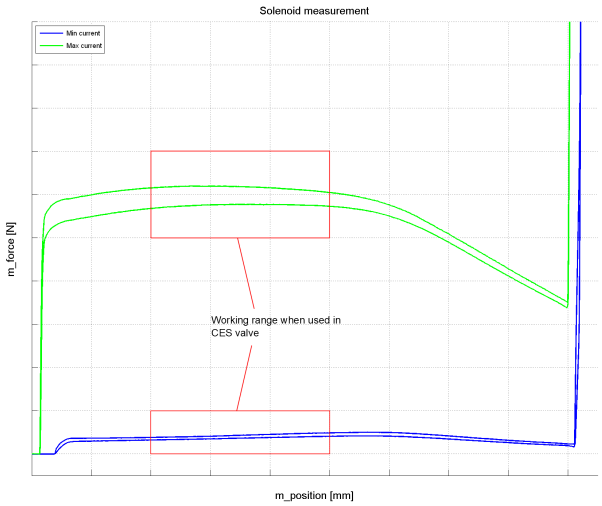

Figure 6.1: Solenoid force at max. (1.6 A) and min. (0.38 A) current

6.2.2 Varying flow coefficient for the pilot orifice

The geometry of the pilot orifice changes as the pilot stage opens. More specifically the ratio between the width and the height of the circular slit changes. Measurements were made to study if the flow coefficient, C_q in equation 2.1, changed due to this change in geometry. During these measurements the pilot poppet was fixed using a screw and its position was measured. Pq-measurements were made for several different positions but unfortunately these measurements were not repeatable. This was due to the fact that the stroke of the pilot poppet is less than 0.1 mm which requires a very high precision when setting and measuring the position.

6.2.3 The orifice P_D

Measurements were made on a custom-made valve to analyse how to model the orifice P_D. This orifice is shown in figure 5.1 and is the inlet to the pilot stage. The entire main stage, pilot shim, pilot spring and pilot poppet were removed on this valve. The outlet for the main flow (through the series orifices) was sealed with a steel ring. This meant that all the flow was forced to go through the orifice P_D.

The measurements showed that the Pq-curve has a non-linear character. P_D was therefore modelled as turbulent and a comparison between simulations and measured data is shown in figure 6.2. The figure shows that the model of the P_D orifice reproduces the pressure drop accurately and is therefore not an uncertain part of the model.

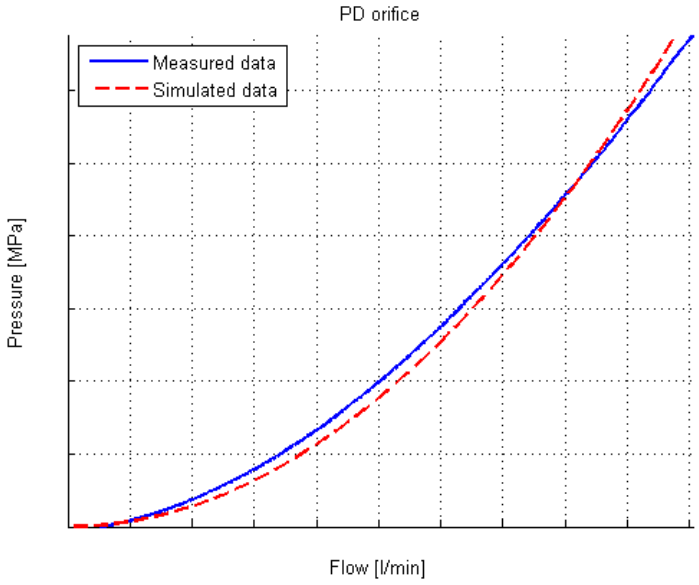

Figure 6.2: Pq-curve for the orifice P_D

6.2.4 Results for the pilot stage model

A comparison between measured and simulated values is shown in figure 6.3 and 6.4. These two configurations represent the extremes with respect to the pressure drop over the pilot stage. Four different solenoid input currents was used to show how accurate the model is at different operating points. A higher current results in a higher pressure drop over the pilot stage.

The pilot stage model gives the best result for the low-pressure configuration and the worst for the high-pressure configuration. Other configurations have been validated as well but none of them showed better or worse fit to measurements than the extreme cases.

Figure 6.4 shows that the slope of the Pq-curve is too low when using the high pressure configuration. A change in valve configuration changes the geometry of the pilot stage, this might cause a change in behaviour that is not captured by the model. The simulation model is accurate for low flow but lacks some precision during high flow.

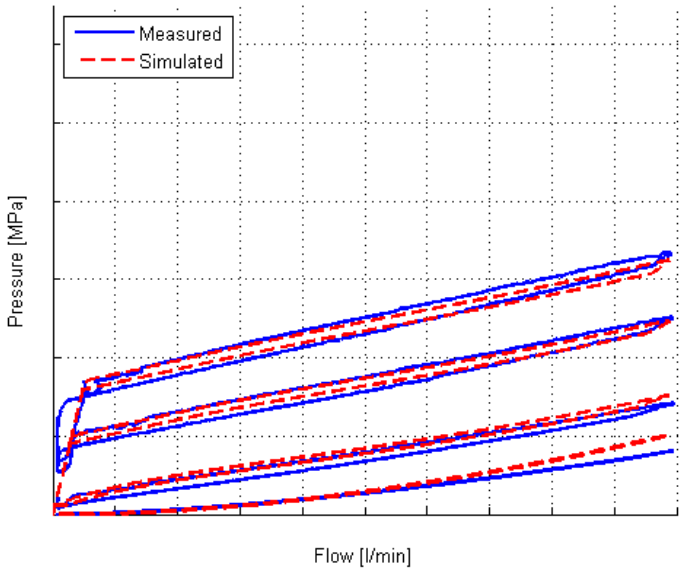

Figure 6.3: Pq-curve for the pilot stage with largest pilot seat and strongest pilot shim

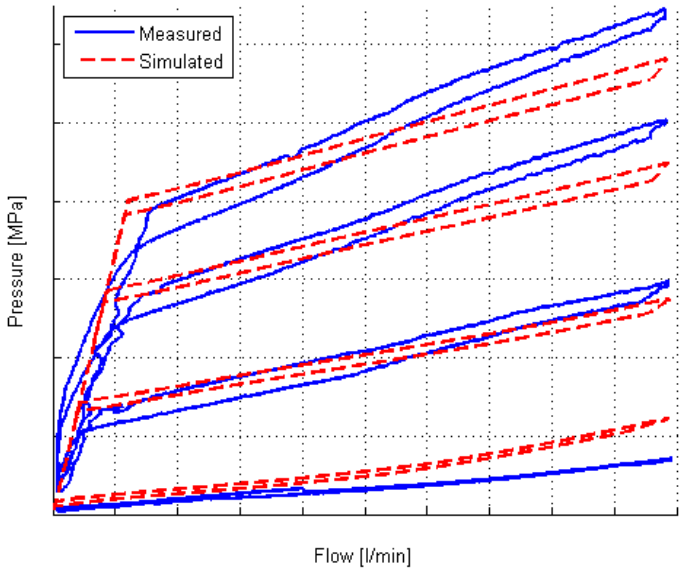

Figure 6.4: Pq-curve for the pilot stage with smallest pilot seat and weakest pilot shim

6.3 Validation of the CES valve model

A validation of the CES valve model is presented in this chapter.

6.3.1 The orifice J_D

Measurements were made on a custom-made valve to validate the orifice J_D which is the orifice through the main poppet (shown in figure 5.5). On this valve the outlet from the main stage was blocked with a steel ring. The entire pilot stage, and the main spring was removed. This forced all the flow to go through the orifice J_D and out through the outlet for the pilot stage.

Figure 6.5 shows the results of the simulation compared to the measurements. The measurements showed that the Pq-curve for J_D is non-linear and J_D was for that reason modelled as turbulent. The figure also shows that the model of the J_D orifice reproduces the pressure drop accurately and is therefore not an uncertain part of the model.

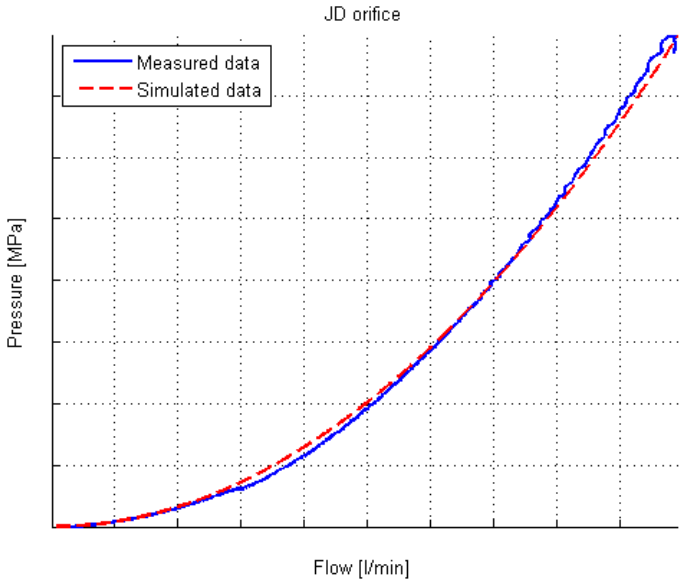

Figure 6.5: Pq-curve for the orifice J_D

6.3.2 The orifice D_S

The orifice D_S is a restrictor used in the flow bench and has been validated against measurements. These measurements were made with a free flow valve instead of the CES valve, making D_S the only orifice that produces a significant pressure drop. The results of the measurements compared to the simulation are shown in figure 6.6. The simulated pressure drop corresponds well with measured data.

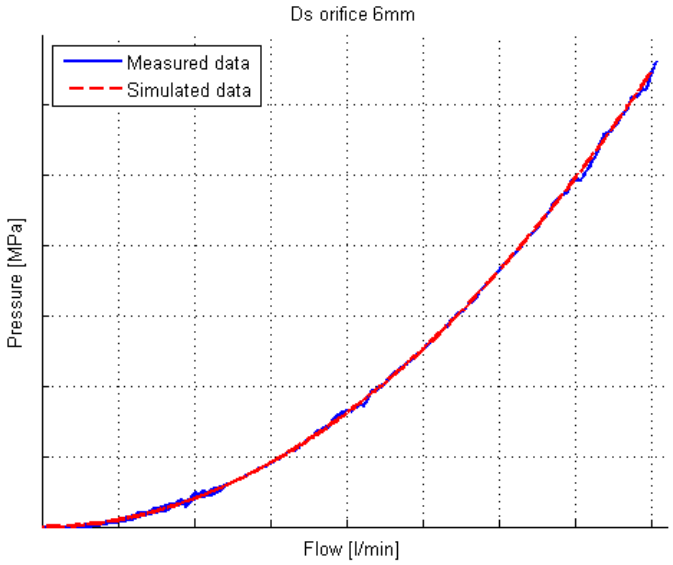

Figure 6.6: Pq-curve for the orifice D_s

6.3.3 Varying flow coefficients for the main stage orifices

Measurements were made with a custom-made valve to determine if and how the flow coefficients varied as a function of poppet position. This time the orifice J_D was sealed and the main poppet was fixed in different positions. This was made by placing shims of different heights under the main poppet, preventing it from moving.

These measurements showed good repeatability and thus was deemed reliable. The flow coefficients for the two main stage orifices was set as a function of the poppet position to fit measured data. The results of using this function are shown in figure 6.7 and the repeatability of the measurements is shown in 6.8. The valve was disassembled and rebuilt before the repetition measurement. These plots show measurements and simulations for the series orifices. The model reproduces the pressure drop accurately and the measurement is repeatable.

6.3.4 Measured flow compared to simulated flow

The flow ramps used when simulating does not look exactly like the actual flow in the flow bench. This difference however has very little effect on the simulation results. The measured and simulated flow are shown in figure 6.9 and the effect it has on the Pq-curve is shown in figure 6.10. The analysis shows that the flow can be simulated in a simplified way without affecting the pressure drop over the CES valve.

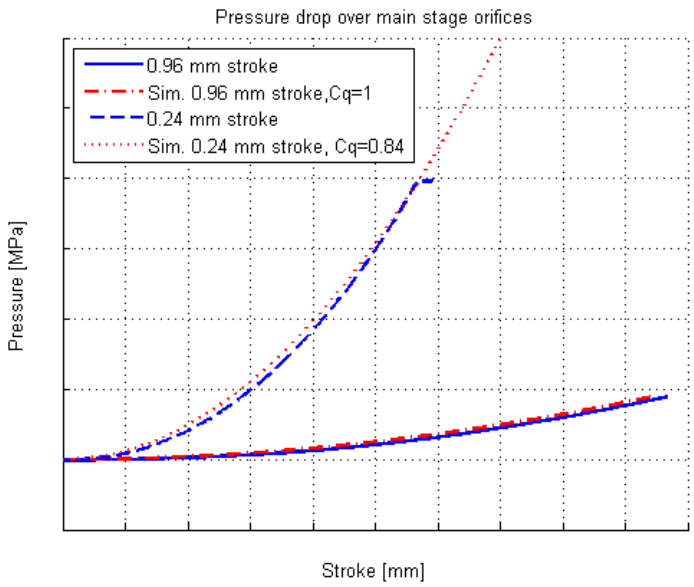

Figure 6.7: Pressure drop over the main stage orifices with fixed poppet

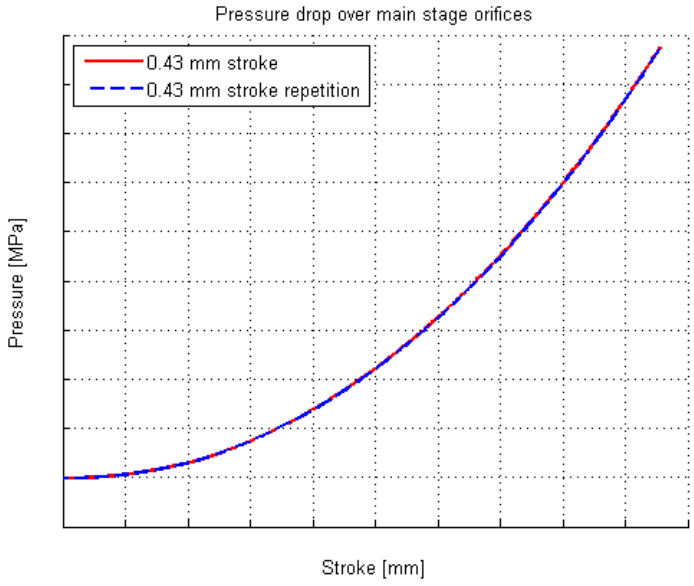

Figure 6.8: Fixed main poppet repeatability

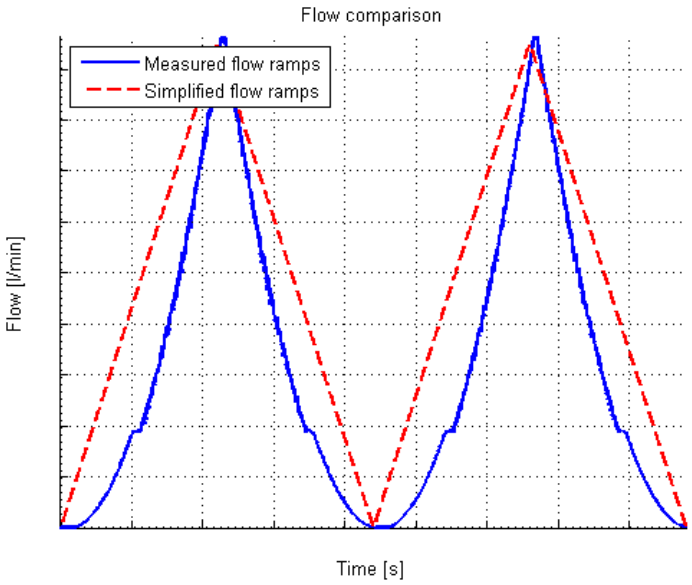

Figure 6.9: Difference between measured and simplified flow

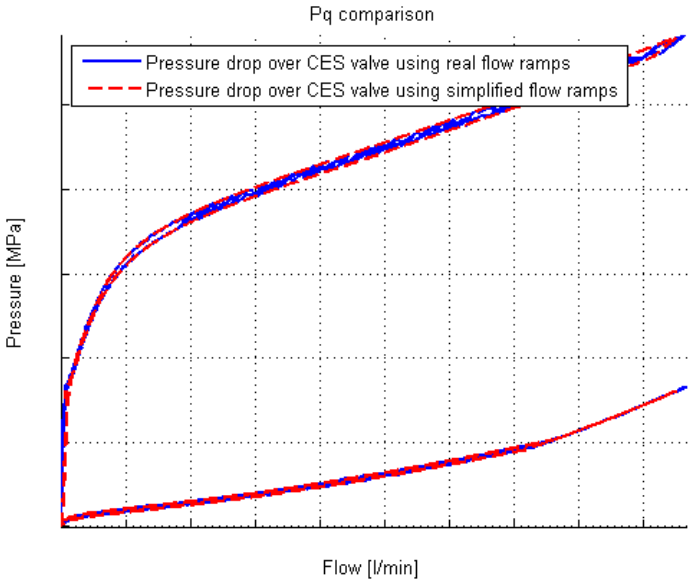

Figure 6.10: Difference in simulation results between using simplified and real flow ramps

6.3.5 Current step during simulations

When doing ASR simulations a simplified version of the real current step was used. This simplification was made in order to achieve a more simple model and to avoid having to retrieve data from external files. This did not affect the results significantly as shown in figure 6.11 and 6.12. The frequency and amplitude of the oscillations that follows the step is not affected by simplifying the current step.

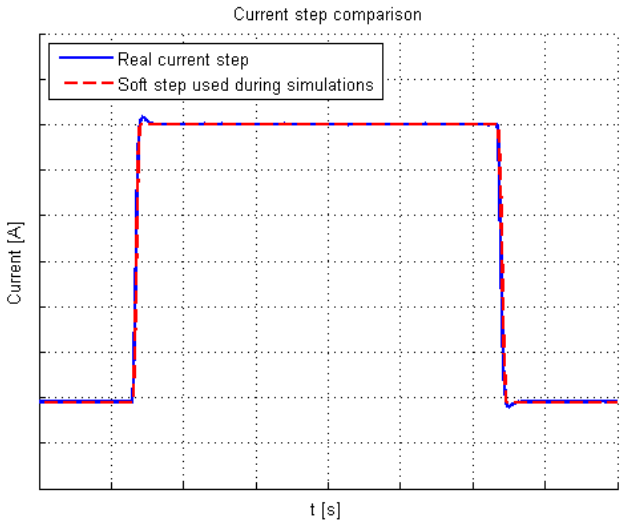

Figure 6.11: Current step during simulations compared to current step during measurements

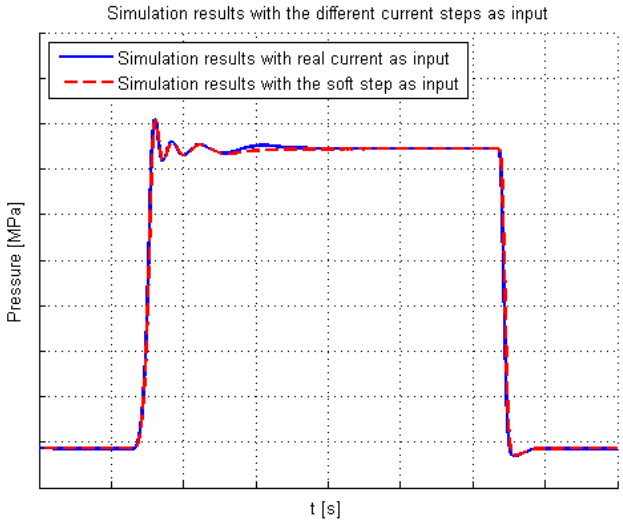

Figure 6.12: Difference in simulation results

6.3.6 Main poppet leak flow

As mentioned earlier in chapter 5 the part of the leak flow due to the main poppet velocity is neglected. This leakage can be calculated according to equation 6.1, where r_{nom} is the nominal radius and h_0 is the narrow gap between the poppet and housing. This leakage is greatest when the velocity is high i.e. during an ASR cycle. The leakage due to poppet velocity can be calculate using equation 6.1 and the velocity from an ASR simulation. This leakage is compared to the leakage due to the pressure difference over the poppet in figure 6.13. The leak flow due to poppet velocity is small compared to the leak flow due to the pressure difference. It is therefore reasonable to neglect the leak flow due to poppet velocity.

$$q_{leak_{velocity}} = \pi v_{mp} r_{nom} h_0 \tag{6.1}$$

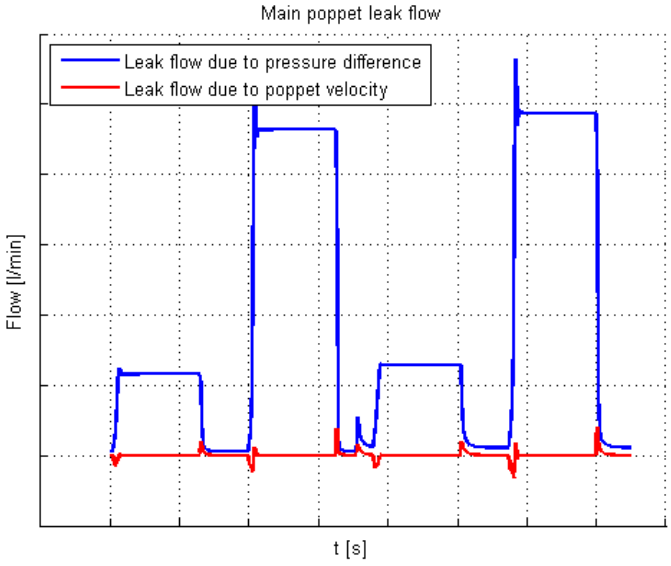

Figure 6.13: Main poppet leak flow

6.3.7 Results for the CES valve model

A comparison between measurement and simulation of two valve types is shown in figure 6.14 and 6.15. These two valve configurations represent the extremes in terms of the pressure drop over the valve. Five different solenoid input currents were used to show how accurate the model is at different operating points during Pq-measurements. A higher current results in a higher pressure drop over the CES valve.

The results when simulating the complete valve show the same trend as in the pilot stage (figure 6.3 and 6.4). The high-pressure configuration gives too low pressure drop at high current in simulations but the low-pressure configuration is more accurate. Improving the pilot stage model would significantly improve the model of the entire CES valve.

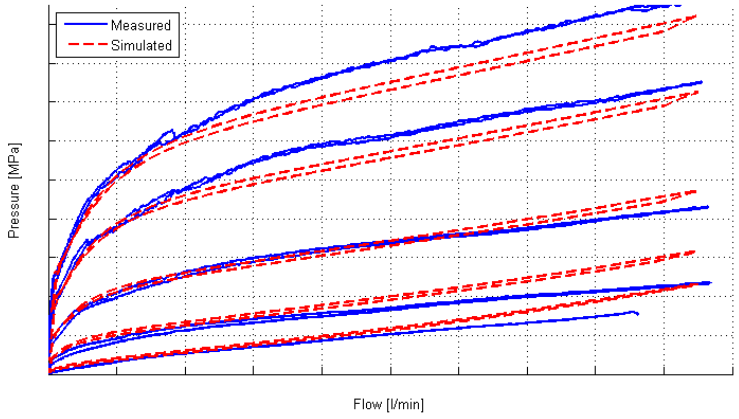

Figure 6.14: Pq-curve for the high-pressure configured CES valve

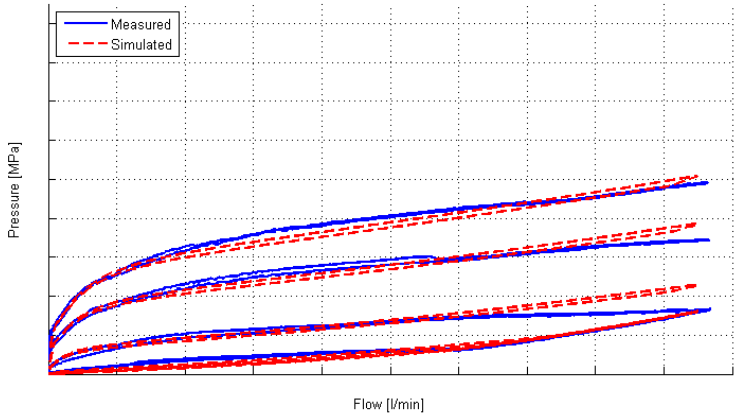

Figure 6.15: Pq-curve for the low-pressure configured CES valve

A validation of the dynamics of the CES valve is shown in figure 6.16 and 6.17. The same valve configurations as in figure 6.14 and 6.15 were used. Current steps were made from 0.38 A to 0.9 A and from 0.38 to 1.6 A while keeping the oil flow constant. The number of oscillations during simulations follow the same trend as during measurements. A configuration that is more oscillative during measurements is more oscillative during simulations as well.

The model captures the rise time and size of the overshoot but not the frequency of the oscillations that follow the step. Obtaining a lower frequency would improve the dynamics of the model.

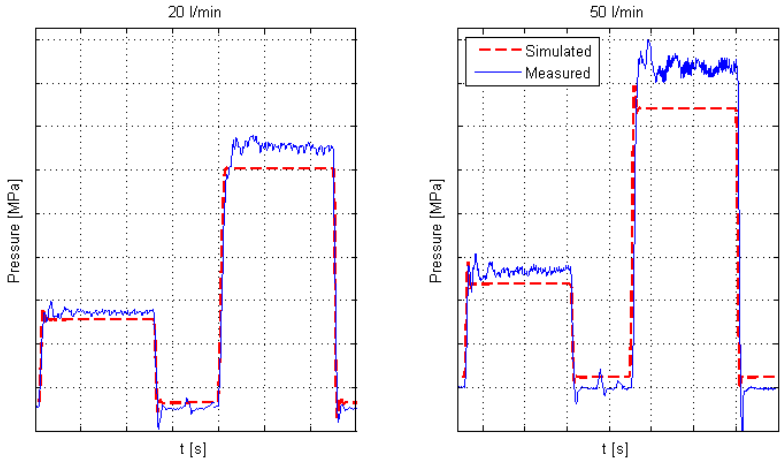

Figure 6.16: Step response for the high-pressure configured CES valve with a flow of 20 or 50 l/min

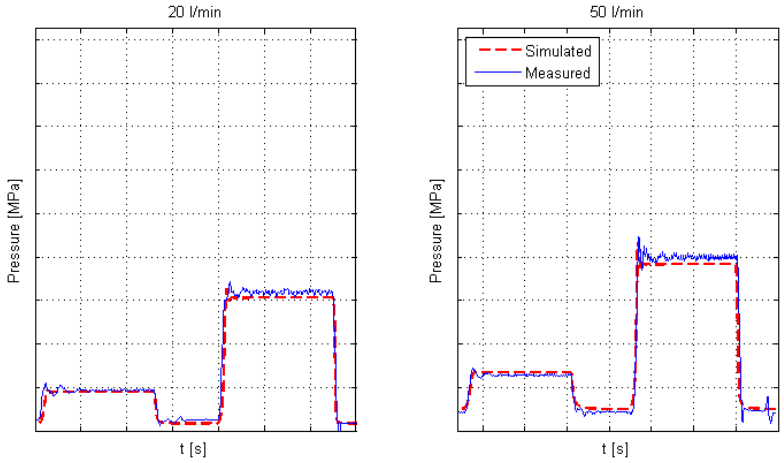

Figure 6.17: Step response for the low-pressure configured CES valve with a flow of 20 or 50 l/min

6.4 Validation of the damper model

A validation of the damper model is presented in this chapter.

6.4.1 Blow-off valves

The blow-off valves of the damper were measured in the flow bench to be able to validate the pressure drop produced by the model.

The blow-off valves were integrated into the complete damper model during the simulations and the result is shown in figure 6.18. The valves show good fit to measurement data but the model of the blow-off valve in the piston is giving unsatisfactory results during its opening phase.

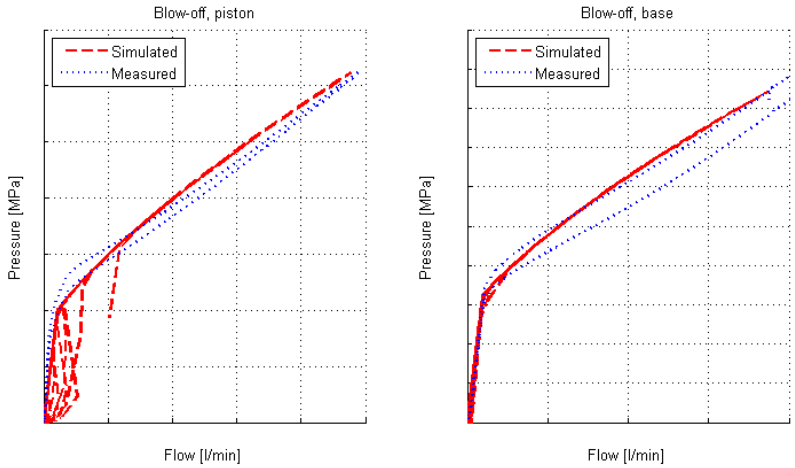

Figure 6.18: Pq-curves for the blow-off valves, measured and simulated data

6.4.2 Check valves

The check valves of the damper were measured in the flow bench to be able to validate the pressure drop produced by the model.

A comparison between measured and simulated data for the check valves is shown in figure 6.19. The check valves were integrated into the complete damper model during the simulations. The model does not capture the opening pressure very well, this can also be seen in figure 6.23. Improving the opening pressure of the check valves would improve the damper model.

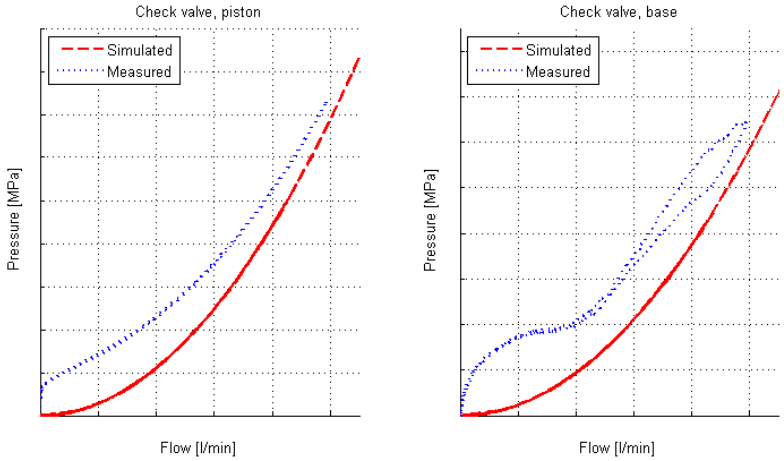

Figure 6.19: Pq-curves for the check valves, measured and simulated data

6.4.3 Gas pressure build-up during a stroke

The maximum stroke of the damper was 5 cm during all measurements in the dynamometer. A stroke with a very low velocity was made to remove any influence from valves and viscous friction. This is shown in figure 6.20 and 6.21.

During this stroke the force caused by the gas pressure build-up is negligible compared to the size of other forces and the measurement noise. It is therefore not necessary to model the gas pressure build-up.

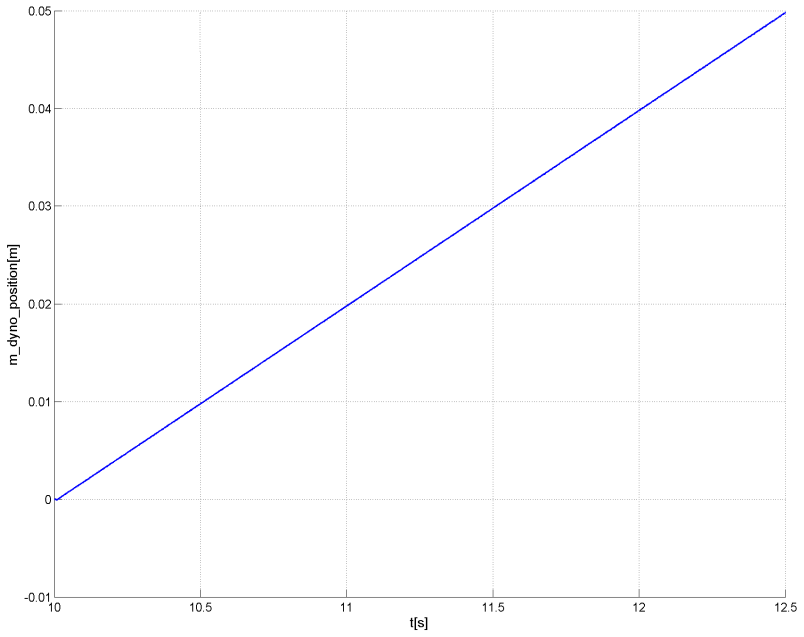

Figure 6.20: Damper stroke when measuring gas pressure force

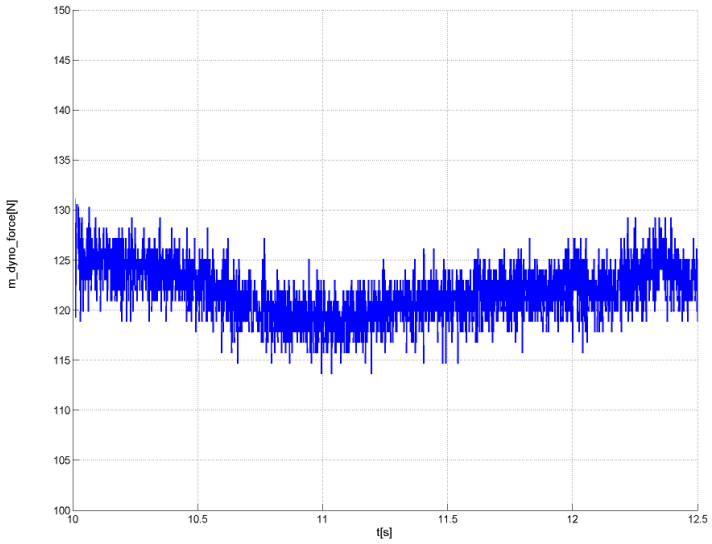

Figure 6.21: Damper force during 5 cm stroke

6.4.4 Results for the damper model

Measurements from the dynamometer were used to validate the damper model. The damper was equipped with a plug or free flow dummy instead of the CES valve. Using a plug means that there is no flow through the ring channel and the blow-off valves in the damper are thereby engaged. The free flow dummy was larger than the built-in restrictor in the damper and thus the behaviour during a free flow measurements is dominated by the check valves. The input to the damper was sine waves with different amplitudes and frequencies according to figure 6.22 where a higher damper velocity produces a higher damping force. The force is positive during compression and negative during rebound.

A comparison between measured and simulated values is shown in figure 6.23 and 6.24. The curves with plugged restrictor shows good fit to measured data which means that the blow-off valves are accurately modelled. However, the free flow curves deviate from measurements, mainly because of the lack of opening pressure in the check valve models.

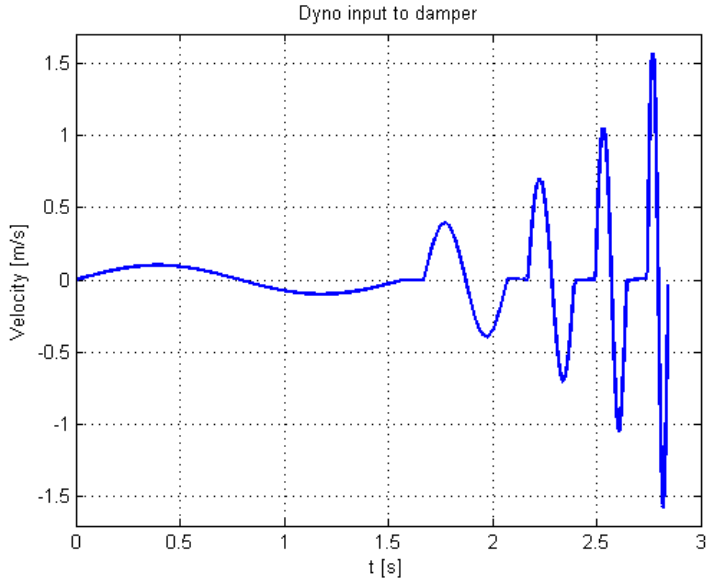

Figure 6.22: Sine wave input to the damper

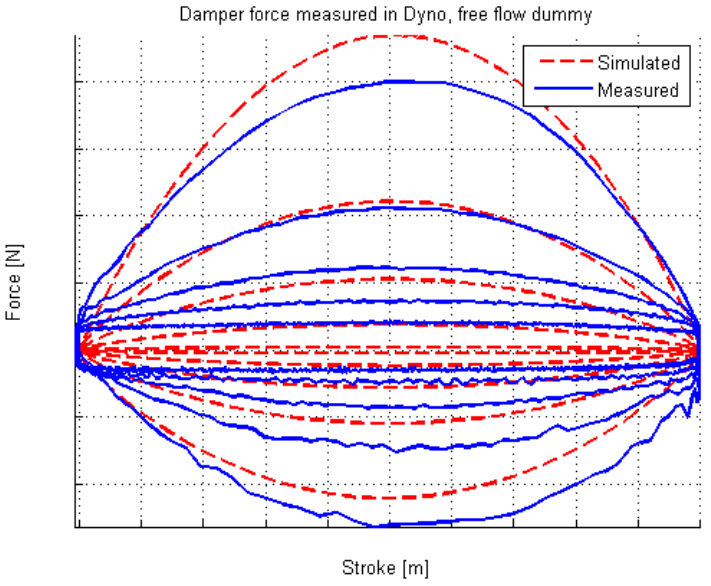

Figure 6.23: Force-stroke, free flow dummy

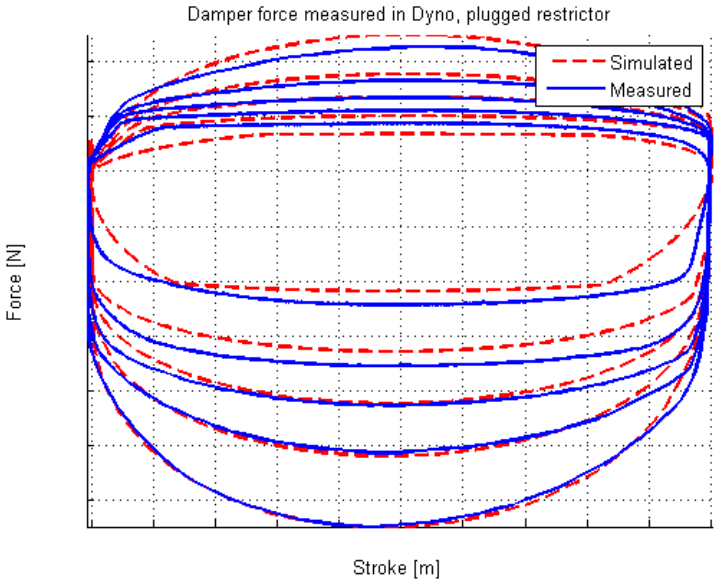

Figure 6.24: Force-stroke, plugged restrictor

6.5 Validation of the flow bench

Due to the fact that the flow bench contains quite a large amount of oil it contributes to the results during dynamic measurements. The dynamics of the flow bench during measurements compared to simulations are shown in figure 6.25. During this measurement and simulation the flow was held constant at 50 l/min while a step in the current from 0.38 A to 1.6 A was performed at 1.147 s and a step down from 1.6 A to 0.38 A was performed at 1.399 s.

The amplitude of the flow oscillations is higher during simulations compared to measurements. This might affect the dynamics of the CES valve model.

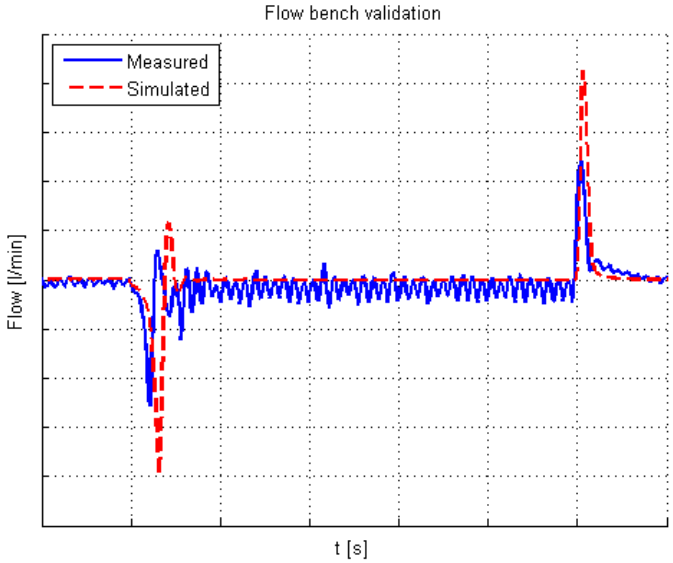

Figure 6.25: Validation of the flow bench

7 Automatic configuration of CES valve

The purpose and theory behind the automatic configuration program is presented in this chapter.

7.1 Purpose of the automatic configuration program

The purpose of the program is to make it possible to analyse the interaction between triple tube dampers and the CES valve. The program should be used to give a recommendation of a suitable valve configuration based on a damping specification for a given damper. The only input needed from the user are measurements on the damper in the dyno with plugged restrictor and free flow dummy along with the piston and rod diameter.

7.2 Estimation of blow-off and check valves from measurements

Pq-curves for the blow off and check valves in the damper are calculated by using equations for the force balance and making assumptions as to how the hydraulic oil flows during different cases. The four different cases are:

- Rebound, free flow dummy
- Rebound, plugged restrictor
- Compression, free flow dummy
- Compression, plugged restrictor

The blow-off valves are assumed to be completely closed during the free flow cases since the forces (and thereby the internal pressure in the damper) are low during these cases. The pressure drop over the check valve in the base was assumed to be zero since the check valves in the base are designed to give a very small flow resistance. Too high resistance in the check valve would lead to cavitation and undesirable characteristics of the damper. A sketch of the damper is shown in figure 7.1, the force F_{damper} is directed as shown in the figure during compression and in the opposite direction during rebound. The absolute value of the damper velocity is used throughout all calculations in this chapter.

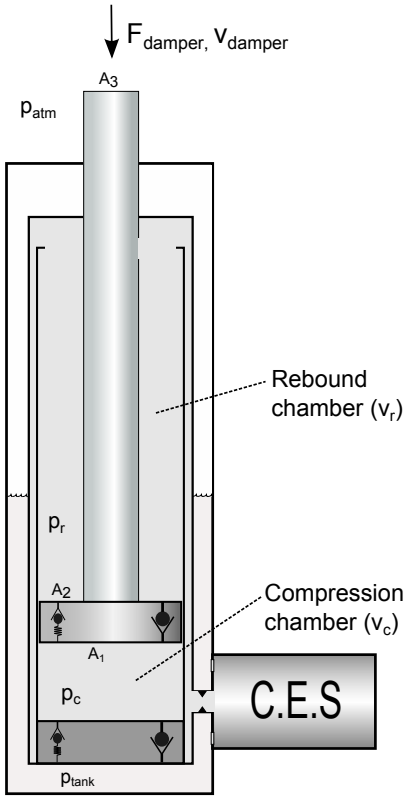

Figure 7.1: Sketch of damper showing the nomenclature

7.2.1 Rebound, free flow dummy

This case was used to calculate an estimation of the pressure drop over the outlet from the inner tube, the ring channel and the restrictor. These three parts are hereafter simply referred to as the restrictor. The pressure in the compression chamber is equal to tank pressure since it is assumed that there is no pressure drop over the check valve in the base.

Setting up the force balance for the piston and solving it for $p_r - p_{tank}$ yields:

$$A_1 - A_2 = A_3 \tag{7.1}$$

$$-p_c A_1 + p_r A_2 + p_{atm} A_3 - F_{damper} = 0 \tag{7.2}$$

$$p_c = p_{tank} \Rightarrow \tag{7.3}$$

$$\Delta p_{restrictor} = p_r - p_{tank} = \frac{F_{damper} + (p_{tank} - p_{atm})A_3}{A_2} \tag{7.4}$$

Assuming a completely closed blow-off valve in the piston gives:

$$q_{restrictor} = v_{damper} A_2 \tag{7.5}$$

A Pq-curve for the flow resistances between the rebound volume and the CES valve was obtained by inserting force-velocity data-pairs in equation 7.4 and 7.5. This data was taken from measurements with a free flow dummy instead of the CES valve.

7.2.2 Rebound, plugged restrictor

This case was used to calculate the pressure drop over the blow-off valve in the piston. Equation 7.6 and 7.7 were used and force-velocity data-pairs were taken from a measurement with a plugged restrictor.

Assuming a completely closed restrictor gives:

$$q_{blowoff,piston} = v_{damper} A_2 \tag{7.6}$$

$$\Delta p_{blowoff,piston} = p_r - p_{tank} = \frac{F_{damper} + (p_{tank} - p_{atm}) A_3}{A_2} \tag{7.7}$$

7.2.3 Compression, free flow dummy

This case was used to calculate a Pq-curve for the check valve in the piston. The force on the piston from the dyno is directed in the opposite direction during compression compared too the rebound case. This yields a force balance according to equation 7.8

$$-p_c A_1 + p_r A_2 + p_{atm} A_3 + F_{damper} = 0 \tag{7.8}$$

Assuming a completely closed blow-off in the base gives:

$$q_{restrictor} = v_{damper} A_3 \tag{7.9}$$

A value for $\Delta p_{restrictor}$ is obtained by inserting the flow calculated using equation 7.9 into the Pq-curve previously calculated for the restrictor. The pressure in the rebound chamber is then calculated according to equation 7.10.

$$p_r = p_{tank} + \Delta p_{restrictor} \tag{7.10}$$

Inserting 7.10 in 7.8 and solving for $\Delta p_{checkvalve,piston} = p_c - p_r$ gives:

$$\Delta p_{checkvalve,piston} = p_c - p_r = \frac{F_{damper} + (p_{atm} - p_{tank} - \Delta p_{restrictor}) A_3}{A_1} \tag{7.11}$$

Completely closed blow-offs yields a flow through the check valve in the piston:

$$q_{checkvalve,piston} = v_{damper} A_1 \tag{7.12}$$

Inserting F-v data-pairs into equation 7.11 and 7.12 gives a Pq-curve for the check valve in the piston.

7.2.4 Compression, plugged restrictor

This case was used to calculate a Pq-curve for blow-off valve in the base of the damper. The flow through the check valve in the piston(equation 7.13) is calculated by assuming no cavitation or pressure build-up in the rebound volume.

$$q_{checkvalve,piston} = v_{damper} A_2 \tag{7.13}$$

The pressure drop over the check valve in the piston ($\Delta p_{checkvalve,piston}$) is calculated by inserting the flow ($q_{checkvalve,piston}$) in the Pq-curve for the check valve in the piston.

The pressure drop over the check valve in the piston can be written according to equation 7.14. Inserting this into the force balance and solving for p_c gives equation 7.15.

$$\Delta p_{checkvalve,piston} = p_c - p_r \tag{7.14}$$

$$p_c = \frac{F_{damper} + p_{atm} A_3 - \Delta p_{checkvalve,piston} A_2}{A_3} \tag{7.15}$$

The Pq-curve can then be calculated from F-v data-pairs by combining equation 7.15, 7.16 and 7.17.

$$\Delta p_{blowoff,base} = p_c - p_{tank} \tag{7.16}$$

$$q_{blowoff,base} = v_{damper} A_3 \tag{7.17}$$

7.3 Calculation of desired pressure drop over CES valve

The desired pressure drop over the CES valve (Δp_{CES}) is calculated by using the Pq-curves for the blow-off and check valves that were calculated in chapter 7.2 and the Force-velocity specification from the customer. This specification typically contains two to seven F-v data-pairs for compression and rebound. An example of a specification is shown in figure 7.2. For the compression side of the graph the higher specification line is a specification of the minimum damping force the damper and CES valve should be able to produce at maximum solenoid current. This is called "Compression hard". The lower curve is a specification of the maximum force the damper and CES valve should produce at the lowest possible solenoid current. This is called "Compression Soft". The same reasoning is used to define "Rebound Hard" and "Rebound Soft".

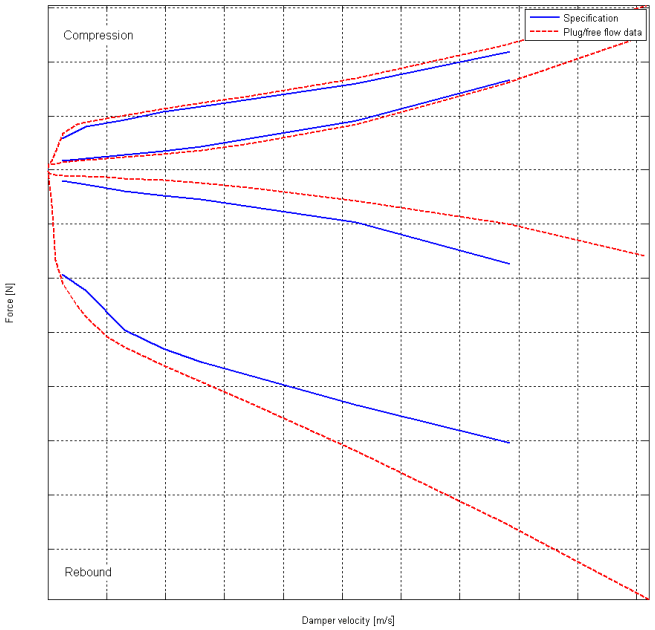

Figure 7.2: Example of a damping specification

7.3.1 Desired Δp_{CES} during compression

For a given damper velocity the total flow out from the compression chamber can be calculated according to equation 7.18. How the flow is divided between the blow-off in the base and the check valve in the piston is unknown and depends on the pressure levels in the damper.

$$q_{tot,cmp} = v_{spec} A_1 \tag{7.18}$$

A number of pressures, p_c, ranging from zero to the maximum calculated pressure for the bottom blow-off ($\vec{p_c} = [0, 100, 200, ..., p_{max}]$ was evaluated. The pressure in the rebound chamber, p_r, was then calculated for each value in $\vec{p_c}$ by using the force balance in equation 7.19.

$$p_{2,cmp} = \frac{p_{1,cmp}A_1 - p_{atm}A_3 - F_{damper_{spec}}}{A_2} \tag{7.19}$$

This yields a number of relationships between the pressure in the compression and rebound chambers and the pressure drops over the active valves (check valve piston and blow off base) are thereby known. By interpolating linearly in the Pq-curves for the flow at a given pressure drop the total flow out from the compression chamber can be calculated by equation 7.20.

$$q_{tot,estimated} = q_{blowoff,base} + q_{checkvalve,piston} \tag{7.20}$$

The pressures p_c, p_r which gives the smallest deviation between the results from equation 7.18 and 7.20 is assumed to be correct. These pressures are then used to calculate the desired pressure drop over the CES valve by using equation 7.21

$$\Delta p_{CES} = p_r - \Delta p_{restrictor} - p_{tank} \tag{7.21}$$

The flow over the CES valve was found by subtracting the flow needed to fill the rebound chamber from the flow through the piston check valve (equation 7.22)

$$q_{CES,cmp} = q_{checkvalve,piston} - v_{spec}A_2 \tag{7.22}$$

7.3.2 Desired Δp_{CES} during rebound

The desired pressure drop over the CES valve during rebound is calculated by first assuming tank pressure in the compression chamber ($p_c = p_{tank}$). The flow out from the rebound volume is found by using equation 7.23.

$$q_{tot,reb} = v_{spec}A_2 \tag{7.23}$$

Inserting $p_c = p_{tank}$ in the force balance gives equation 7.24

$$p_{2,reb} = \frac{p_{tank}A_1 - p_{atm}A_3 + F_{damper_{spec}}}{A_2} \tag{7.24}$$

The desired pressure drop over the CES valve was then found by using equation 7.21 and the corresponding flow by using equation 7.25

$$q_{CES,reb} = q_{tot,reb} - q_{blowoff,piston} \tag{7.25}$$

The calculations in chapter 7.3.2 were made with F-v data-pairs from measurements with plugged restrictor or a free flow dummy to obtain Rebound Hard and Soft curves.

7.4 Validation of automatic configuration program

This chapter contains a validation of the estimation of the internal valves and the calculation of the desired CES Pq-curve.

7.4.1 Estimation of valves

A damper was measured in the dyno to obtain Force/velocity data with plugged and free flow dummy. The equations in chapter 7.2 were used to calculate estimations of Pq-curves for the valves and restrictor in the damper. The flow through the valves and thus the range of the estimated curves is determined by the velocity of the damper during the measurements along with piston and rod areas. A damper of the same kind as the one used for measurements in the dyno was then disassembled and the individual valves were measured in the flow bench. A comparison between estimations and measurements is shown in figure 7.3 and 7.4.

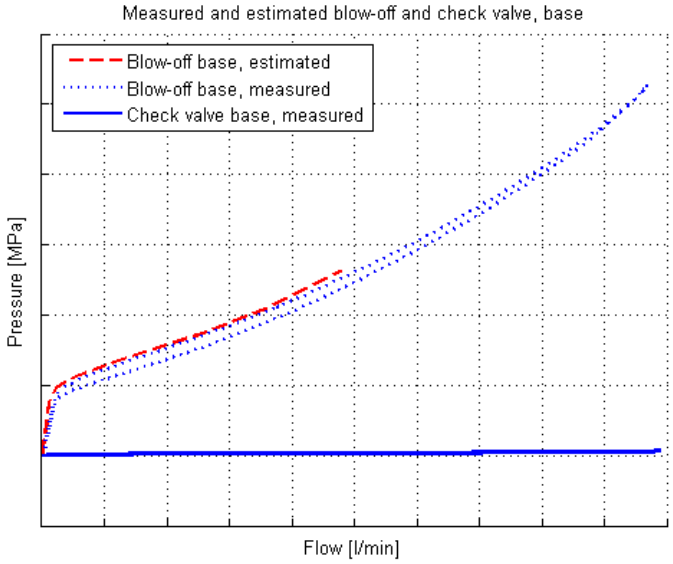

Figure 7.3: Comparison between measured and estimated Pq-curves for the valves in the base

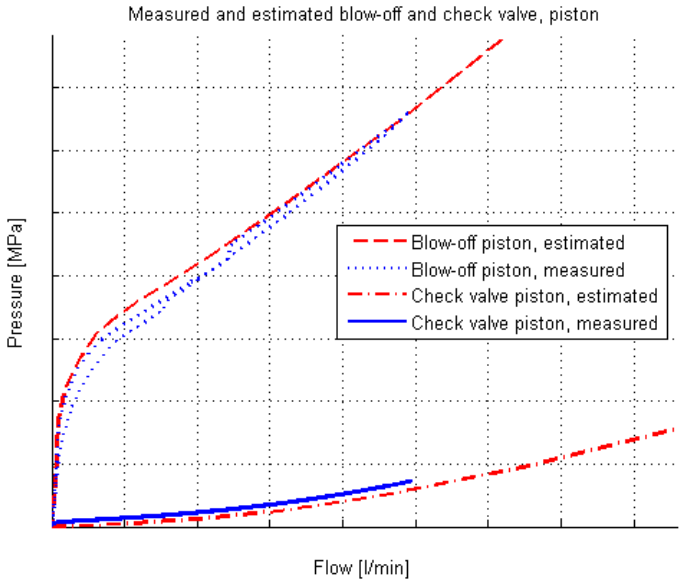

Figure 7.4: Comparison between measured and estimated Pq-curves for the valves in the piston

7.4.2 Calculation of desired CES Pq-curve

The damper was equipped with a CES valve and run in the dyno using two different currents, 0.35 A and 0.8 A. The measured forces and velocities were then used as a damping specification in the configuration program. With a perfect calculation of the desired CES curve this would lead to a desired curve that looks exactly like the Pq-curve for the given valve at the specified currents. The valve has been measured in the flow bench at these currents and a comparison is shown in figure 7.5. The calculated pressure drop is roughly 10% lower than the actual pressure drop.

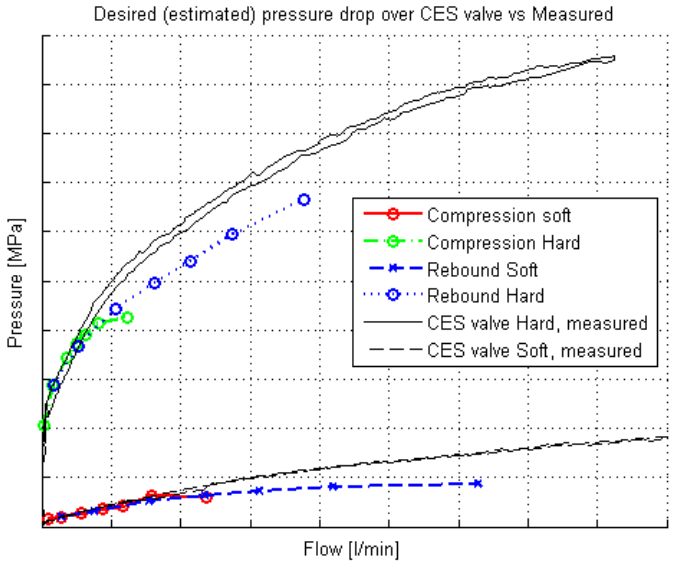

Figure 7.5: Comparison between measured and calculated pressure drop over the CES valve

7.5 Least-squares optimization

The least-squares method is used to evaluate the difference between the desired Pq-curve for the CES valve and the simulated curves. The desired Hard and Soft curves are compared to simulations with maximum and minimum solenoid current respectively. The least-squares optimization is executed for the velocities in the damping specification and the valve configuration with the smallest total weighted error is chosen.

7.6 The graphical user interface

A user interface was developed using MATLAB to simplify usage of the configuration program. The interface gives the possibility to input a damping specification and to weight the different data-points. The most suitable valve configuration is presented along with Pq-curves for the CES valve. A screenshot of the user interface is shown in figure 7.6.

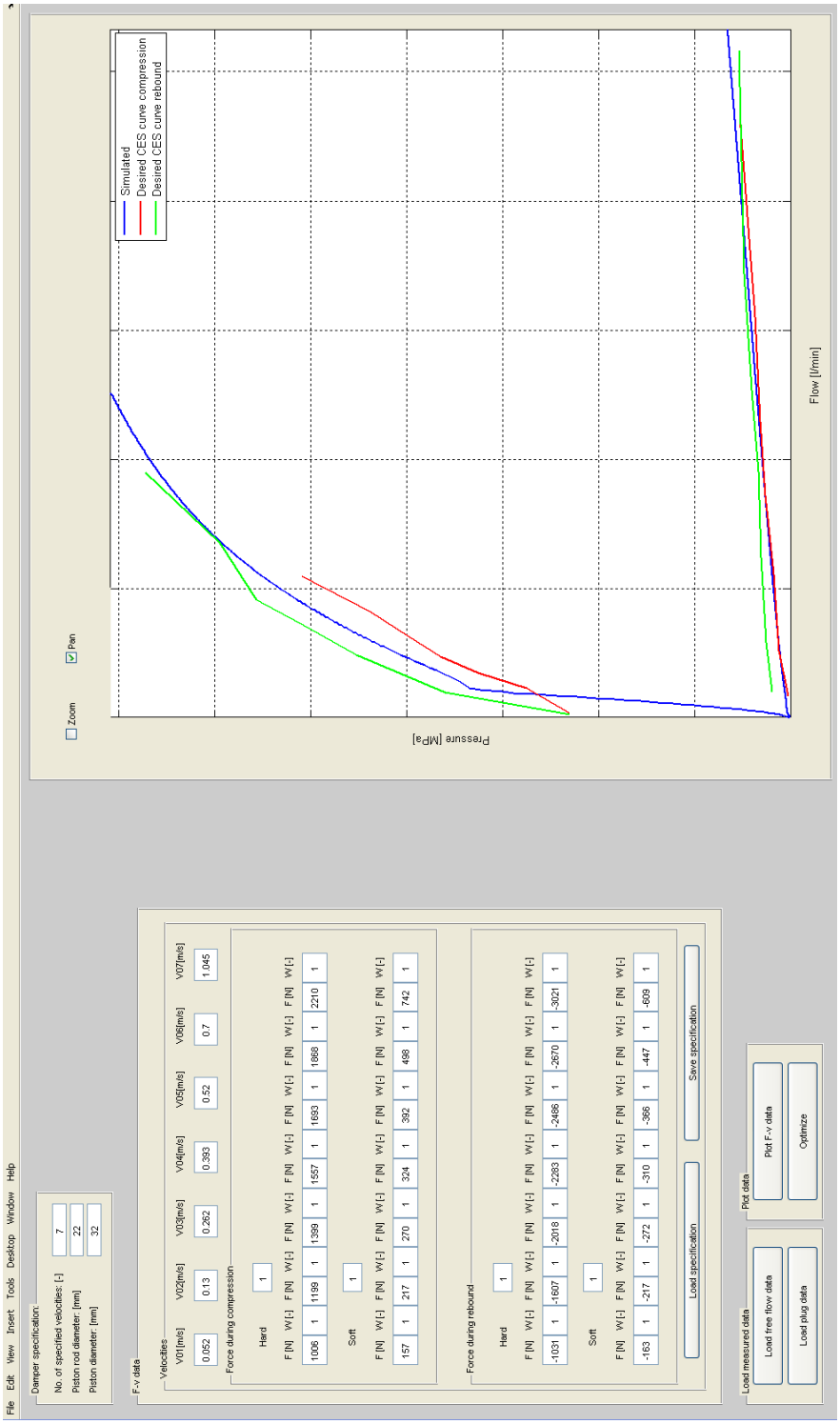

Figure 7.6: Screenshot showing the user interface

8 Conclusions

A short summary of the work performed during this thesis project is presented in this chapter. The main uncertainties of each sub-model is discussed further in chapter 9.

8.1 The CES valve

Literature regarding modelling and hydraulic valves were studied in order to gain more knowledge about similar systems. The behaviour of the CES valve was then studied by generating a simulation model using Hopsan. The model was split into two modules, the pilot stage and the main stage.

8.1.1 Pilot stage

The pilot stage model is focused around the pilot poppet, the model considers mechanical forces in the form of spring forces and an applied force from the solenoid. The electromagnetic solenoid force is a static function of input current that is derived from measurements. It also considers hydraulic forces including for example flow forces and viscous friction. The flow coefficient for the pilot orifice was modelled as a function of the poppet position.

The model was validated, for different valve configurations, against static measurements in a flow bench. Results show that the simulations correspond well to the measurements for low-pressure valve configurations but deviates more for high-pressure configurations.

The main uncertainties of the pilot stage model are the flow forces, the pressurised area in the pilot orifice and the model of the flow coefficient.

8.1.2 Main stage

The main stage model is focused around the main poppet and is similar to the pilot stage model in the sense that it considers flow forces, variable flow coefficient and viscous friction. There is no externally controlled force in the main stage model but it models mechanical forces from springs.

Measurements cannot be made on the main stage without using a pilot stage, therefore the complete CES valve model was validated. Static and dynamic measurements were used when validating. The simulations correspond well to the static measurements for low-pressure configurations but, similarly to the pilot stage, deviates more for the high-pressure configurations. This is an error that propagates from the pilot stage model. Dynamic measurements, i.e. step responses, showed that the model captures the rise time and the size of the pressure overshoot well. However, it doesn't reproduce the correct frequency of the oscillations that follow the step.

In the main stage model it was possible to validate the flow coefficient model but some uncertainties still remain. The main ones are the pressurised area of the series orifices and the flow forces.

8.2 The damper

The damper that was studied and modelled was a triple tube (uniflow) damper which contains four internal valves. No drawings or data for the damper was available which meant that parameters, for example spring rates, had to be guessed. The optimization function in Hopsan was used to set the parameters by comparing to measurements in the flow bench. These measurements were critical to the outcome of the model as they made it possible to validate each internal valve individually.

Both of the blow-off valves show good fit to measurements while the check valves lack opening pressure. Improving the check valve models would improve the damper model significantly. A validation of the complete damper model was made against measurements in the dynamometer. The damper model showed good fit to measurements when using a plugged restrictor but not as good with a free flow dummy. These results confirm that more work is needed with the model of the check valves.

8.3 The automatic configuration program

A method of estimating the characteristics of the internal valves of a triple tube damper was developed. These estimations are used to calculate a desired pressure drop over the CES valve given a damping specification. The calculated pressure drop is then compared to simulations of the CES valve in order to choose the most suitable valve configuration. The program was built using MATLAB and has graphical user interface. The user provides the necessary input through the interface and is presented with the results from the calculations.

The estimation of the blow-off and check valves was validated against measurements in the flow bench, this showed that the estimations correspond well to measurements. The flow bench was also used to validate the calculated pressure drop over the CES valve. The validation showed that the calculation was about 10% lower than measurements.

9 Discussion

A discussion about uncertainties and areas that need improvement is given in this chapter.

9.1 The CES valve model

This section contains a discussion regarding the model of the CES valve.

9.1.1 Deviation among the valves

The fact that there is a deviation in behaviour among the valves has to be taken into consideration when validating the model. This deviation is due to measurement uncertainty, assembling differences and distribution within the tolerances. Ideally a large amount of measurements should be used to calculate a mean value to which the model should be fitted. This would mean a lot of work due to the fact that these valve individuals would have to come from different batches and the valves would also have to be disassembled and reassembled several times.

Shown in figure 9.1 is an interval of two standard deviations for 30 individuals of the same valve configuration, the simulation results for that same configuration is also shown. An interval of two standard deviations means that, if the measurements are normally distributed, 95% of the measurements are found within this interval. The simulation result of this valve configuration is within the interval for high current but lacks in precision for lower currents. It also shows that the choice of measurement when validating is of importance.

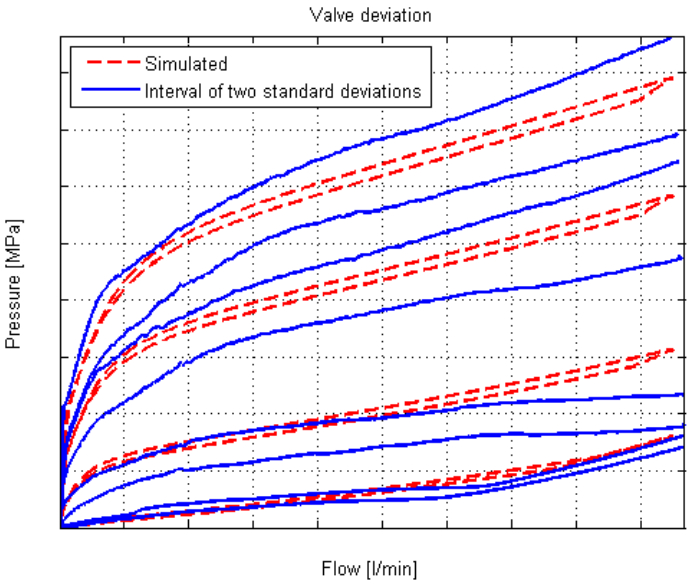

Figure 9.1: Deviation among 30 valves

9.1.2 Pressure distribution in the pilot orifice

The pressure distribution in the pilot orifice is important to get a correct pressure level in the CES valve. A sensitivity analysis was made to show the difference between the smallest and largest possible pressurised areas in pilot orifice. Pressurising to the inner radius means that there is no pressure in the slit. This is shown in figure 9.2 where the valve current is 1.6 A. The effect of these radii for the complete CES valve model is shown in figure 9.3. It is obvious that the pressurised area is of paramount importance to the simulation result.

The best simulation results were achieved by pressurizing about 44.1% of the slit radius ($r_{slit_{pp}}$). A CFD (Computational Fluid Dynamics) analysis of the slit could possibly give a better understanding of the pressure distribution and which radius to use.

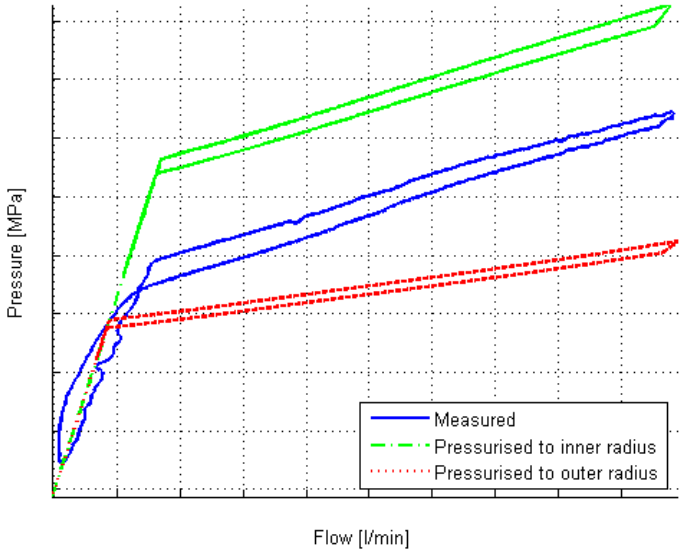

Figure 9.2: Difference in pressure level between largest and smallest radius

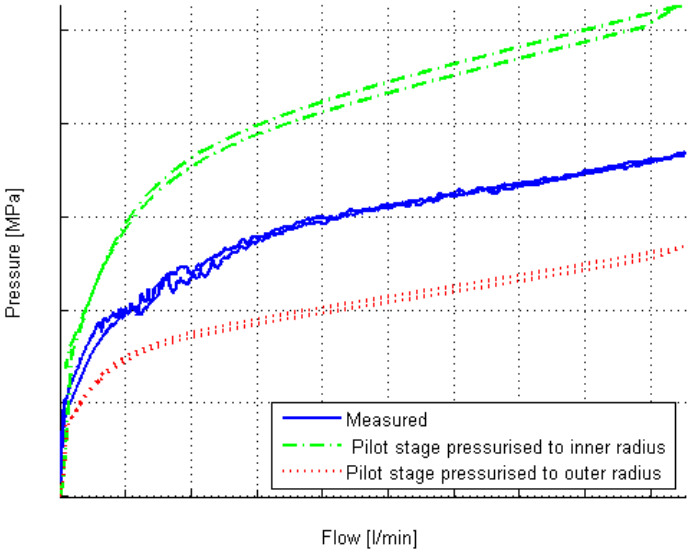

Figure 9.3: Difference in pressure level in the main stage using largest and smallest radius in the pilot stage

9.1.3 Pressure distribution in the main stage orifices

A study similar to the one above was carried out for the main stage by changing the pressurised areas in the main stage. No pressure in the axial, annular slits would lead to a pressurised area according to the upper part of figure 9.4. The other extreme, fully pressurised slits, is shown in the bottom half of the figure.

The results in pressure levels, at 1.6 A current, is shown in figure 9.5. This shows that the impact of changing the pressurised areas in the main stage is significant but not as large as for the pilot stage.

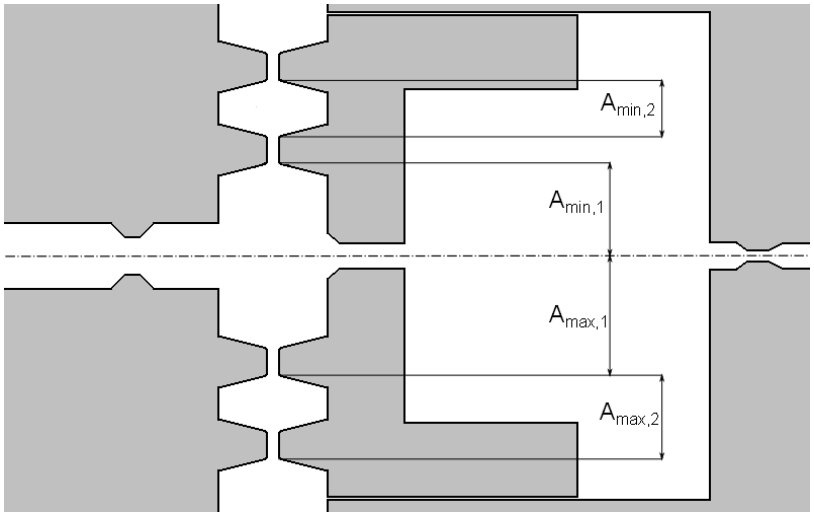

Figure 9.4: Explanation of min/max pressurised areas in the main stage

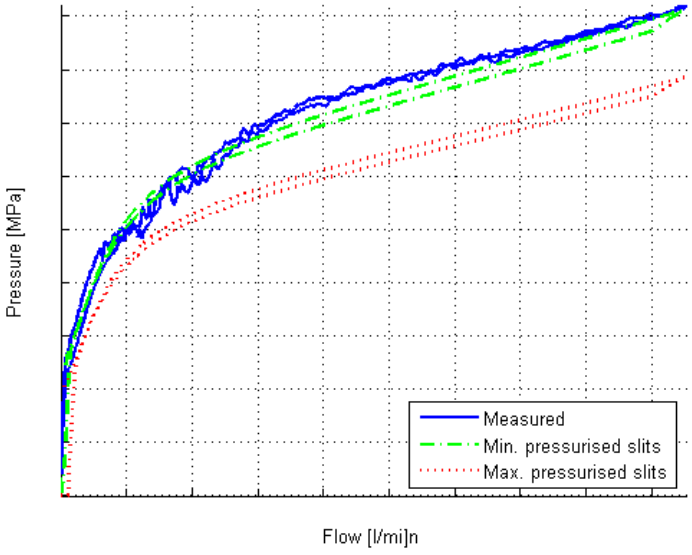

Figure 9.5: Difference in pressure level between maximum and minimum pressurised areas

9.1.4 Flow forces

The flow forces, which are closing the valve, are difficult to calculate analytically. The main uncertainty is the flow angle which defines how much the fluid changes direction. A sensitivity analysis was made to show how big impact the flow forces have on the pilot and main stage. The angle was set to zero (maximum flow forces) and 90° (no flow forces). The difference between these extremes is shown in figure 9.6, 9.7 and 9.8. The configuration that gives the highest pressure drop over the CES valve was used during this comparison.

This analysis shows that the flow forces have a significant influence during high pressure both in the pilot and main stage. From these figures it would be easy to draw the conclusion that maximum flow forces should be used, however that causes too high pressure drop when using the configuration that gives the lowest pressure drop over the CES valve.

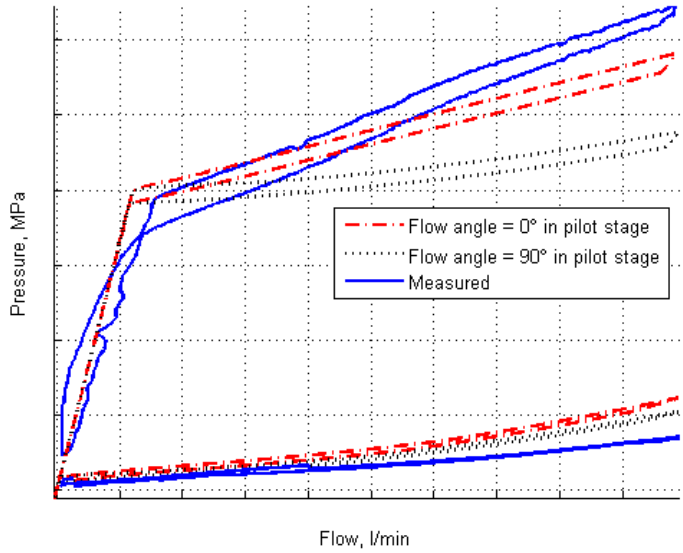

Figure 9.6: Difference in pressure level for the pilot stage with maximum/zero flow forces in the pilot stage model

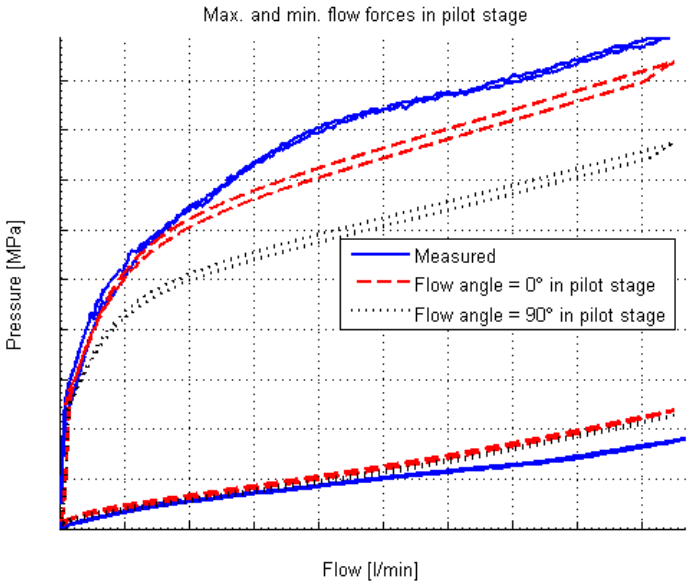

Figure 9.7: Difference in pressure level for the CES valve with maximum/zero flow forces in the pilot stage model

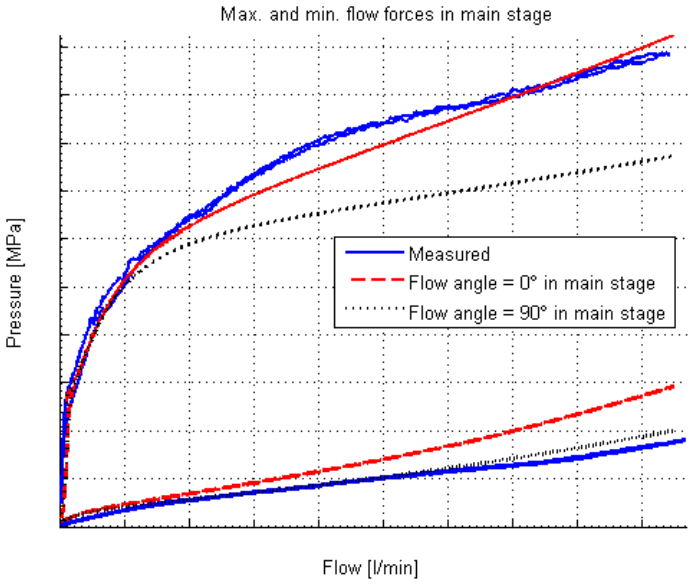

Figure 9.8: Difference in pressure level for the CES valve with maximum/zero flow forces in the main stage model

9.1.5 The pilot diameter's effect on Cq and flow forces

The pilot diameter is one of the configuration parameters for the valve. Changing it does not change the fundamental geometry of the pilot stage but still results in a slight change in the geometry. This might cause the flow coefficient C_q to change as well as the beam angle δ for the flow forces. This is something to take into consideration for future work.

9.1.6 Pilot orifice flow coefficient

Attempts were made to fix the pilot poppet at a specific position but coming up with a reliable way of doing this was not possible. Measurements made on the main stage showed that the flow coefficient varied as a function of the main poppet position (chapter 6.3.3). It was therefore assumed that the pilot orifice flow coefficient changed as a function of the pilot poppet position. The function that defines the flow coefficient (figure 5.2) was created to get better agreement with measurement data. A CFD analysis is probably needed to verify the accuracy of the model of C_q.

9.1.7 Flow bench dynamics

There is a small deviation in the flow bench dynamics between the model and reality. The amplitude of the flow-oscillations during a current step is larger in the model compared to measurements, as shown in figure 6.25. This means that the model of the flow bench has a greater dampening effect than the real flow bench. If the flow bench in the model was made stiffer and more accurate it would probably lead to a slightly larger overshoot in pressure when performing ASR simulations.

9.1.8 Solenoid dynamics

The model of the solenoid doesn't include any dynamics, a third-order polynomial that is fitted to measurement data is used. It has been indicated in [6] that the dynamics of the solenoid are important to the dynamic response of solenoid controlled valves. Creating a more advanced model of the solenoid could possibly improve the dynamics of the CES model.

9.1.9 Solenoid friction

Measured and modelled friction in the solenoid is shown in figure 9.9, the model deviates from measurements. The friction was initially modelled according to measurements but this resulted in too much hysteresis in the pilot stage model. The model of the friction was tuned so that it fitted better with Pq-measurements for the pilot stage. The large hysteresis during the solenoid measurements might be due to the fact that the solenoid wasn't pressurised, which it is when used in a CES valve.

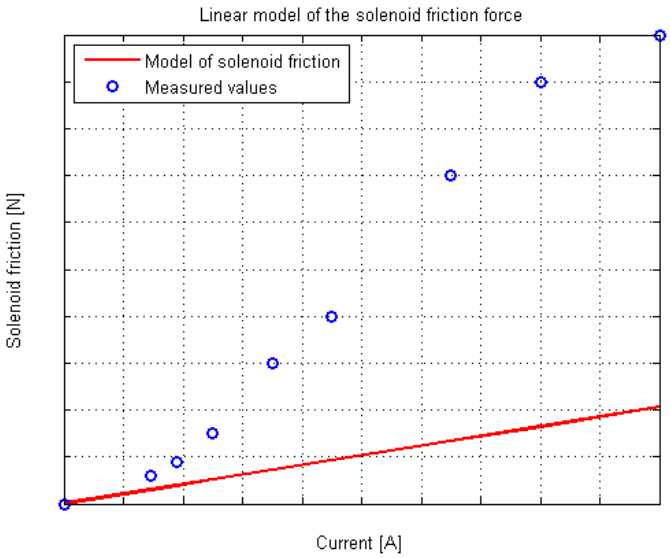

Figure 9.9: Solenoid friction, modelled and measured

9.2 The damper model

The damper model presented in this thesis is still in its infancy and further development is needed to get accurate results when simulating it together with the CES valve. Suggestions as to where the model can be improved is found hereinafter.

9.2.1 Blow-off valves

The blow-off valves were initially modelled separate from the damper and tuned against measurements from the flow bench. This way it was possible to tune each valve individually before inserting them into the complete model. Some further tuning had to be done after inserting them due to the fact that the valve dynamics and the interaction between the valves and the damper came into play. The damping orifice in the model of the massless poppet valve is critical for the dynamics of the blow-off models.

9.2.2 Check valves

The check valves were also initially modelled and tuned separate from the damper but showed to be tougher to tune after insertion into the model. Their opening pressure is too low which has an impact on the results when simulation the damper with a free flow dummy. The initial force needed to move the damper (about 60 N) is partially created by mechanical friction (15-20 N) but the remaining force is probably due to the opening pressure of the check valves. An improvement of the check valves and especially their opening pressure would significantly improve the damper model. See figure 6.23.

9.2.3 Viscous friction

It has been hard to get good results for both compression and rebound at the same time whilst modelling the damper. This has led to the conclusion that it might be necessary to model it with different viscous friction in compression and rebound. It is also possible that proper tuning of the check valves might solve this problem.

9.2.4 Mechanical friction

The dynamometer controls the damper by giving velocity, in the form of sine-waves, as input. It was desired to have the same type of input in the simulation model in order to mimic the measurements as closely as possible. Controlling a mass with a velocity source is unfortunately not possible in Hopsan and masses are, as of now, the only component which simulates mechanical friction. This friction is a significant part of the force which is required to move the damper at low velocity and is therefore of importance to the simulation model. Attempts were made to include mechanical friction by using signal components but this resulted in instability.

If a cylinder with mechanical friction is added to Hopsan or a way to control a mass using velocity is developed this problem could easily be solved.

9.3 The automatic configuration program

The initial plan was to use the damper model when choosing the most appropriate valve. This was changed when it became obvious that tuning a damper model is very time-consuming and a good model requires disassembly of the damper. The chosen method gives a result in much shorter time and does only require basic knowledge of the damper geometry. The damper is not produced by Öhlins Racing AB and little is therefore known about the internal dimensions and tolerances of the damper.

The estimations off the blow-off valves give a pressure drop that is roughly 10% higher than the measurements (see figure 7.3 and 7.4). The deviation from measurements is of the same magnitude when calculating the desired CES curve.

The automatic selection of valve configuration will most likely not be the end to all valve-selection problems and is only one small part in the puzzle when choosing a final valve configuration. It does however give a valuable insight into the flow and pressure levels for the given damper.

A Models in Hopsan

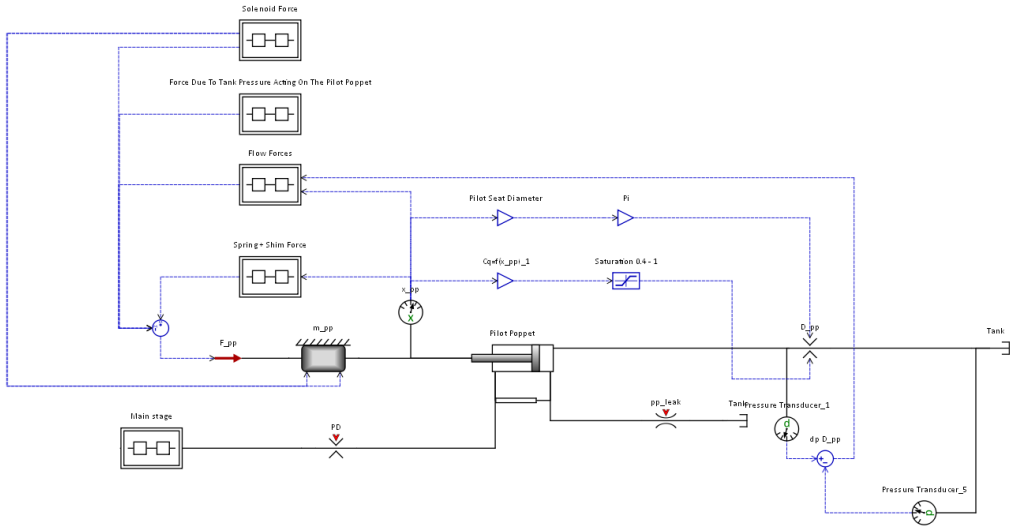

Figure A.1: The pilot stage model

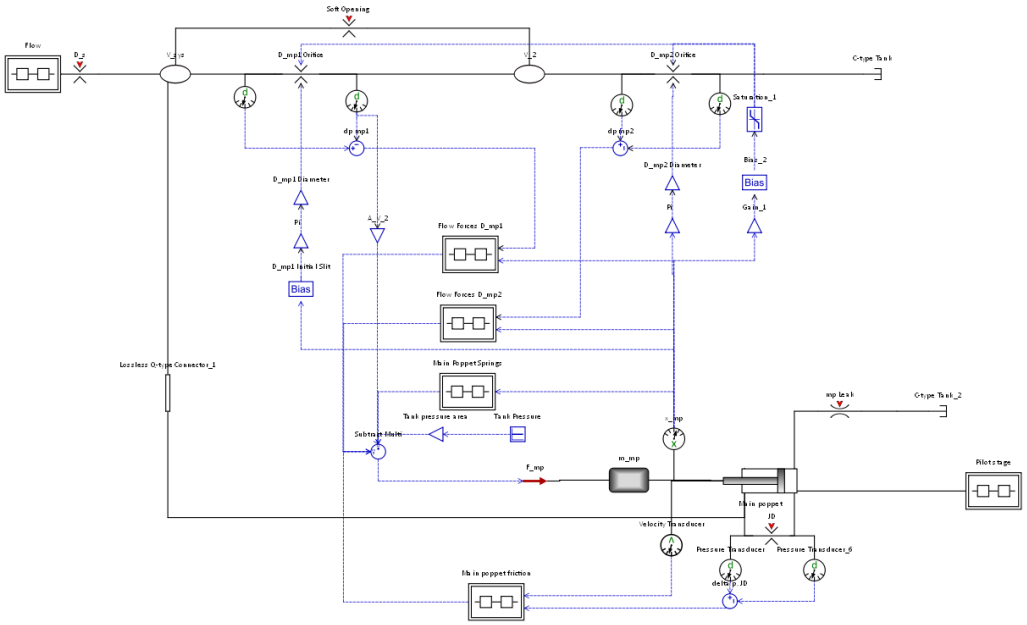

Figure A.2: The main stage model

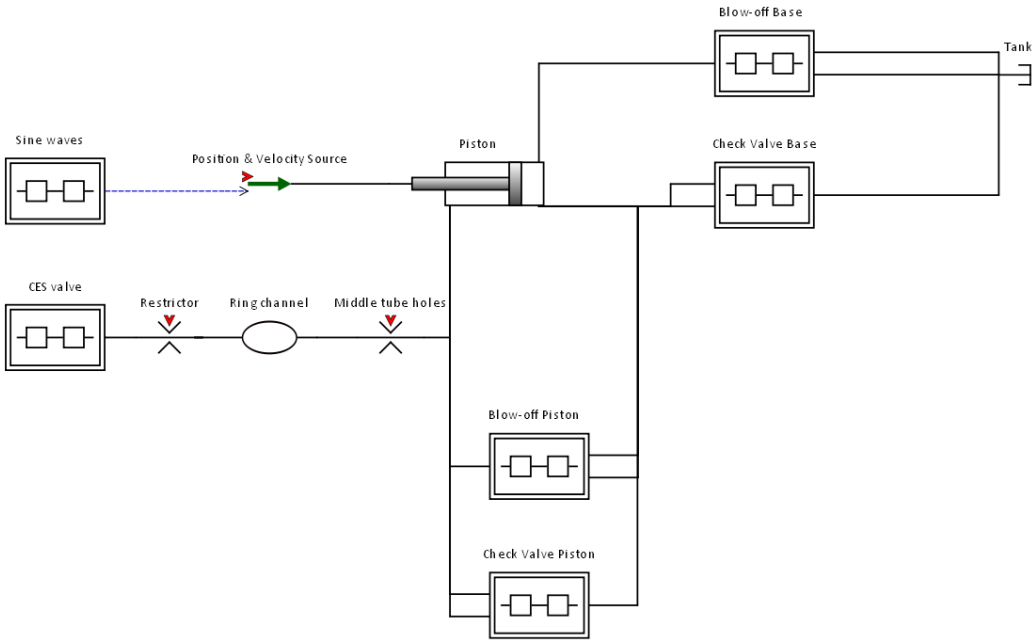

Figure A.3: The damper model

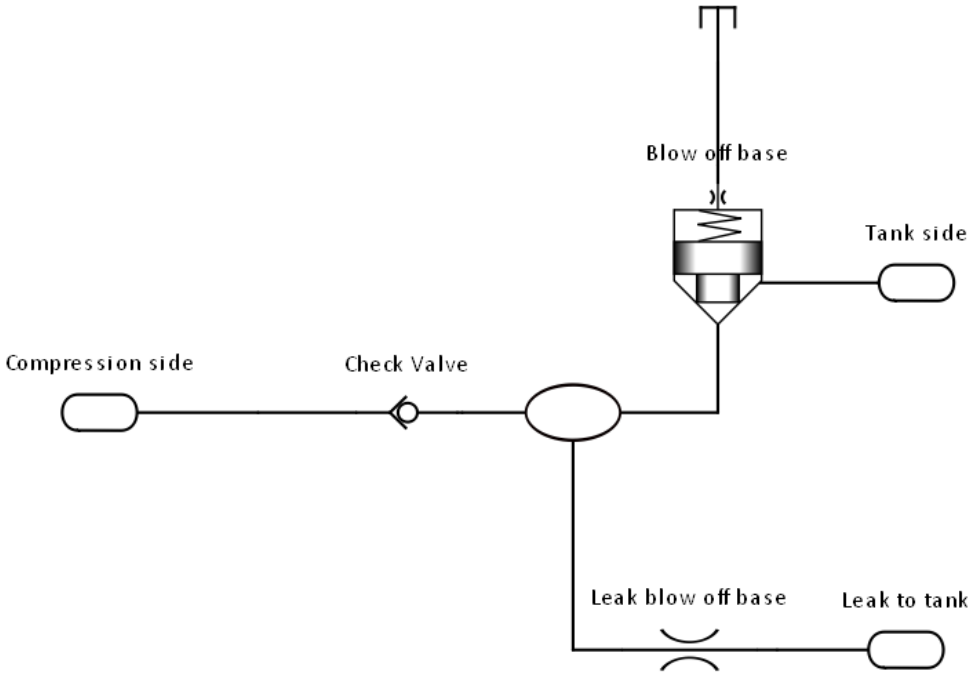

Figure A.4: The model of a blow-off valve in Hopsan (check valves are modelled in the same way)

B Nomenclature

$\Delta p_{blowoff,base}$	Pressure drop over the blow-off valve in the damper base
$\Delta p_{blowoff,piston}$	Pressure drop over the blow-off valve in the damper piston
Δp_{CES}	Pressure drop over the CES valve
$\Delta p_{checkvalve,piston}$	Pressure drop over the check valve in the damper piston
$\Delta p_{restrictor}$	Pressure drop over the restrictor in the damper
η	Dynamic viscosity of the oil
A_{mp_1}	Pressurised area of the main poppet in the volume V_sys
A_{mp_2}	Pressurised area in the volume V_2
A_{mp}	Pressurised area within the main poppet
A_{soft}	Soft opening slit area
A_1	Damper piston area
A_2	Damper ring area (piston area - piston rod area)
A_3	Damper piston rod area
$A_{q_{mp1}}$	Flow area of the inner main stage orifice
$A_{q_{mp2}}$	Flow area of the outer main stage orifice
$A_{q_{pp}}$	Flow area of the pilot orifice
D_s	Flow bench restrictor
F_{damper}	Damper force
$F_{hyd_{mp}}$	Hydraulic force acting on the main poppet
$F_{hyd_{pp}}$	Hydraulic force acting on the pilot poppet
F_{sol}	Solenoid force
h_0	Gap between main poppet and housing
i_{sol}	Solenoid current
J_D	Orifice through the main poppet
k_{mp}	Main spring rate
k_{shim}	Pilot shim rate
l_{mp}	Length of the main poppet
m_{mp}	Main poppet mass
m_{pp}	Pilot poppet mass
n	Number of residuals
p_{atm}	Atmospheric pressure
p_{tank}	Tank pressure
$p_{V_{mp}}$	Pressure in the volume V_{mp}
$p_{V_{sys}}$	Pressure in the volume V_{sys}
p_{V_2}	Pressure in the volume V_2
p_c	Pressure in the compression chamber
P_D	Pilot stage inlet orifice
p_r	Pressure in the rebound chamber

$q_{blowoff,base}$	Flow through the blow-off valve in the base
$q_{blowoff,piston}$	Flow through the blow-off valve in the piston
$q_{CES,cmp}$	Flow through the CES valve during compression
$q_{CES,reb}$	Flow through the CES valve during rebound
$q_{checkvalve,piston}$	Flow through the check valve in the piston
$q_{leak,coeff}$	Leakage coefficient for the leakage over the main poppet
$q_{leak_{velocity}}$	Leakage over the main poppet due to the velocity of the poppet
q_{mp}	Main flow
q_{pp}	Pilot flow
$q_{restrictor}$	Flow through the restrictor
$q_{tot,cmp}$	Total flow out of the compression chamber
$q_{tot,estimated}$	Calculated total flow out of the compression chamber
$q_{tot,reb}$	Total flow out of the rebound chamber
r_{mp}	Main poppet housing radius
r_{mp1}	Radius to the inner edge of the inner main stage orifice
r_{mp2}	Radius to the inner edge of the outer main stage orifice
r_{nom}	Main poppet nominal radius
r_{pp}	Pilot seat radius
$r_{slit_{mp}}$	Main orifice width
$r_{slit_{pp}}$	Pilot orifice width
r_{sol}	Solenoid rod radius
r_i	Residual
S	Total error during least squares calculation
v_{damper}	Damper velocity
V_{mp}	Volume within the main poppet
v_{mp}	Main poppet velocity
V_{sys}	Volume between D_s,J_D and the main stage inner orifice
V_2	Volume between the two main stage orifices
V_c	Damper compression chamber volume
W_i	Weight of the residual
V_r	Damper rebound chamber volume
x_{mp}	Main poppet position
x_{pp}	Pilot poppet position

References

[1] Institutionen för konstruktions- och produktionsteknik, Linköpings tekniska högskola, "Formelsamling i Hydraulik och pneumatik", 1995

[2] Krus, Jansson, Palmberg och Weddfeldt , "Distributed Simulation of Hydromechanical Systems"

[3] http://www.iei.liu.se/flumes/system-simulation/hopsanng?l=en, 2012-01-11

[4] Jonas Ek, "Stabilitetsanalys av stötdämparventil", 2007

[5] F. Selin, M. Svensson, "Svängningar i ventiler för semiaktiva dämpare", 2010

[6] K. Dasgupta, J. Watton, "Dynamic analysis of proportional solenoid controlled piloted relief valve by bondgraph", 2004

[7] Carrera Akutain, X., Viñolas, J., Savall, J. and Biera, J. (200x) "A parametric damper model validated on a track", Int. J. Heavy Vehicle Systems

[8] P. Krus, D. Teien, "Modelling and simulation methodology for the human cardio vascular system",2001

[9] P. Krus, M. Karlsson, J. Engvall, "Modelling and simulation of the human arterial tree using transmission line elements with visco-elastic walls", 1991

[10] Yuming Hou, Lingyang Li, Ping He, Yunqing Zhang, Liping Chen, "Shock Absorber Modeling and Simulation Based on Modelica", 2011

[11] W. Durfee, Z. Sun, "Fluid Power System Dynamics", 2009

[12] R. Chahine, "Modeling of a World Rally Championship Car Damper and Experimental Testing of Its Components",2011